A homeostatic interferon-lambda response to bacterial microbiota stimulates preemptive antiviral defense within discrete pockets of intestinal epithelium

Authors: Jacob A. Van Winkle [1], Stefan T. Peterson[2], Elizabeth A. Kennedy[2], Michael J. Wheadon[2], Harshad Ingle[2], Chandni Desai[3], David A. Constant[1], Austin P. Wright[1], Lena Li[1], Maxim Artyomov[3], Sanghyun Lee[2], Megan T. Baldridge[2,4#], and Timothy J. Nice[1#]

Affiliations:

[1] Department of Molecular Microbiology and Immunology, Oregon Health and Science University, Portland, OR, 97239, USA

[2] Division of Infectious Diseases, Department of Medicine, Edison Family Center for Genome Sciences & Systems Biology, Washington University School of Medicine, St. Louis, MO 63110, USA

[3] Division of Immunobiology, Department of Pathology and Immunology, Washington University School of Medicine, St. Louis, MO 63110, USA

[4] Department of Molecular Microbiology, Washington University School of Medicine, St. Louis, MO 63110, USA

[#]Correspondence to: nice@ohsu.edu (T.J.N.), mbaldridge@wustl.edu (M.T.B.)

Abstract

Interferon-lambda (IFN-λ) protects intestinal epithelial cells (IECs) from enteric viruses by inducing expression of antiviral IFN-stimulated genes (ISGs). Here, we find that bacterial microbiota stimulate a homeostatic ISG signature in the intestine of specific pathogen-free mice. This homeostatic ISG expression is restricted to IECs, depends on IEC-intrinsic expression of IFN-λ receptor (*Ifnlr1*), and is associated with IFN-λ production by leukocytes. Strikingly, imaging of these homeostatic ISGs reveals localization to pockets of the epithelium and concentration in mature IECs. Correspondingly, a minority of mature IECs express these ISGs in public single-cell RNA sequencing datasets from mice and humans. Furthermore, the bacterial component, lipopolysaccharide, partially restores localized ISGs in mice lacking bacterial microbiota. Lastly, IECs lacking *Ifnlr1* are hyper-susceptible to initiation of murine rotavirus infection. These observations indicate that bacterial microbiota stimulate ISGs in localized regions of the intestinal epithelium at homeostasis, thereby preemptively activating antiviral defenses in vulnerable IECs to improve host defense against enteric viruses.

31 **Introduction**

32 Interferons (IFNs) are a family of cytokines produced in response to infection that signal
33 IFN receptor-bearing cells to induce transcription of hundreds of interferon-stimulated genes
34 (ISGs). These ISGs perform diverse functions, but many cooperate to induce an antiviral state
35 (Sadler and Williams, 2008; Schoggins and Rice, 2011). There are three types of IFNs: type I
36 IFNs (IFN-αs, IFN-β, others), type II IFN (IFN-γ), and type III IFNs (IFN-λs). These three types are
37 differentiated by receptor usage (type I IFN receptor: *Ifnar1*/*Ifnar2*; type II IFN receptor:
38 *Ifngr1*/*Ifngr2*; type III IFN receptor: *Ifnlr1*/*Il10rb*), but all three receptor complexes signal through
39 Janus-kinase (JAK) and signal transducer and activator of transcription (STAT) factors to
40 stimulate ISG transcription (Ingle et al., 2018; Schneider et al., 2014). Type I and III IFNs are
41 directly stimulated by host detection of microbe-associated molecular patterns (MAMPs) such as
42 viral nucleic acids, and the prominent contribution of these IFN types to antiviral defense is
43 reflected by the breadth of evasion strategies used by diverse viral families to prevent their
44 production or action (Levy and García-Sastre, 2001; Rojas et al., 2021; Taylor and Mossman,
45 2013). The type I IFN receptor is expressed broadly across most cell types, whereas the type III
46 IFN receptor, *Ifnlr1,* is primarily restricted to epithelial cells (Kotenko and Durbin, 2017;
47 Sommereyns et al., 2008). Accordingly, IFN-λ is of particular importance in effective antiviral
48 defense of barrier tissues.

49 Interestingly, previous studies in mice have noted that intestinal epithelial cells (IECs) are
50 hyporesponsive to type I IFN (Lin et al., 2016; Mahlakõiv et al., 2015; Pott et al., 2011; Van Winkle
51 et al., 2020). Additionally, infection of mice deficient in IFN receptors (*Ifnar1*, *Ifngr1*, *Ifnlr1*; single
52 or double knockouts) with enteric viruses indicates that IFN-λ is the predominant antiviral IFN type
53 that controls viral replication in the gastrointestinal epithelium (Mahlakõiv et al., 2015; Nice et al.,
54 2015; Pott et al., 2011). IECs can robustly respond to IFN-λ with upregulation of canonical antiviral
55 ISGs and increased resistance to infection by enteric viruses, such as rotaviruses and noroviruses

56 (Baldridge et al., 2017; Nice et al., 2015; Pott et al., 2011). Mouse rotavirus (mRV) is a natural
57 pathogen of mice that infects enterocytes located at the tips of villi in the small intestine (Burns et
58 al., 1995). Rotaviruses have developed mechanisms to antagonize the induction of IFN by
59 infected cells, suggesting that evasion of the IFN response is necessary for efficient epithelial
60 infection (Arnold et al., 2013). Indeed, prophylactic administration of IFN-λ significantly reduces
61 the burden of mRV infection, demonstrating its potential for mediating epithelial antiviral immunity
62 to this pathogen (Hernández et al., 2015; Lin et al., 2016; Pott et al., 2011; Van Winkle et al.,
63 2020). However, a protective role of the endogenous IFN-λ response to mRV infection is less
64 clear, perhaps reflecting the success of mRV evasion mechanisms.

65 Epithelial immunity in the gut must be appropriately balanced to protect the intestinal
66 epithelium while preventing loss of barrier integrity and intrusion by microbes that are abundant
67 within the gastrointestinal tract. The bacterial microbiota in the intestine perform critical functions,
68 aiding in host metabolism (Krajmalnik-Brown et al., 2012), providing a competitive environment
69 to defend against pathogens (Kim et al., 2017), and initiating and maintaining host immune
70 function during homeostasis (Honda and Littman, 2016; Rooks and Garrett, 2016). In this complex
71 environment host epithelial and immune cells detect bacteria and viruses using a suite of pattern
72 recognition receptors (PRRs) that sense the presence of MAMPs. Stimulation of PRRs, such as
73 the toll-like receptor (TLR) family, activates antimicrobial and antiviral defenses providing local
74 protection in many tissues (Chu and Mazmanian, 2013; Iwasaki and Medzhitov, 2015; Thompson
75 et al., 2011). TLR-dependent pathways induce production of IFNs, primarily by signaling through
76 TIR-domain-containing adapter-inducing interferon-β (TRIF) and myeloid differentiation primary
77 response 88 (MYD88) adapter proteins (Monroe et al., 2010; Odendall et al., 2017), providing a
78 mechanism by which bacterial MAMPs can initiate IFN responses.

79 Signals from the bacterial microbiota have been shown to elicit a steady-state type I IFN
80 response in systemic tissues and cell types that can prime antiviral immunity by several
81 independent studies (Abt et al., 2012; Bradley et al., 2019; Ganal et al., 2012; Steed et al., 2017;

82 Stefan et al., 2020; Winkler et al., 2020). Additionally, a steady-state ISG signal has been
83 observed in the intestine of uninfected mice (Baldridge et al., 2015; Lin et al., 2016; Stockinger et
84 al., 2014), but this intestinal response remained poorly characterized. Together with the observed
85 hypo-responsiveness of IECs to type I IFN, these findings suggested that bacterial microbiota
86 may stimulate a local IFN-λ response in the gut. To explore this interaction, we undertook the
87 present study to assess the role of bacterial microbiota in induction of enteric ISGs at homeostasis
88 using a combination of broad-spectrum antibiotics (ABX) and genetically modified mice.

89 In this study, we uncovered an ISG signature in IECs that was dependent on the presence
90 of bacteria and IFN-λ signaling (hereafter referred to as 'homeostatic ISGs'). This panel of genes
91 was present in WT mice with conventional microbiota and was reduced in WT mice treated with
92 ABX and in mice lacking *Ifnlr1*. We revealed that homeostatic ISG expression is i) restricted to
93 the intestinal epithelium across both the ileum and colon, ii) independent of type I IFN signaling,
94 and iii) associated with IFN-λ transcript expression by epithelium-associated CD45+ leukocytes.
95 Surprisingly, we found that homeostatic ISGs are not expressed uniformly by all IECs; rather,
96 expression is concentrated in localized pockets of IECs and in differentiated IECs relative to crypt-
97 resident progenitors. These patterns of localized ISG expression are corroborated by
98 independently-generated single-cell RNA sequencing data from mouse and human IECs. We also
99 found that ISG expression can be partially rescued by reconstitution of bacterial microbiota or
100 administration of bacterial lipopolysaccharide (LPS) to ABX-treated mice. Finally, we found that
101 this microbiota-stimulated ISG signature provides protection from initiation of mRV infection.
102 Cumulatively, this study found that bacteria initiate preemptive IFN-λ signaling in localized areas
103 to protect IECs from enteric viruses.
104

105 **Results**

106 **Bacterial microbiota stimulate IFN-λ response genes in the ileum at homeostasis**

107 To determine the effect of bacterial microbiota on homeostatic IFN-λ responses, we
108 compared gene expression in whole ileum tissue for the following experimental groups: i) wild-
109 type C57BL/6J (WT) mice intraperitoneally-injected with IFN-λ as compared to unstimulated WT
110 mice, ii) WT mice with conventional microbiota as compared to WT mice treated with an antibiotic
111 cocktail (ABX) to deplete bacteria, iii) WT mice with conventional microbiota as compared to *Ifnlr1*$^{-}$
112 $^{/-}$ mice with conventional microbiota, and iv) *Ifnlr1*$^{-/-}$ mice with conventional microbiota compared
113 to *Ifnlr1*$^{-/-}$ mice treated with ABX (**Figure 1A**). We performed gene-set-enrichment-analysis
114 (GSEA) to test for enrichment or depletion of 'IFN-λ response genes' that were defined in a prior
115 study of IFN-λ-stimulated ileum tissue (Lee et al., 2019). As expected, GSEA comparing IFN-λ-
116 treated WT mice to unstimulated WT mice showed significant enrichment of IFN-λ response
117 genes (**Figures 1B-C**). Therefore, GSEA of these genes is indicative of IFN-λ responses in the
118 ileum and GSEA can be used to assess the relative differences in IFN-λ responses between
119 experimental conditions.

120 To deplete bacterial microbiota, we administered a cocktail of broad-spectrum antibiotics,
121 and demonstrated that this treatment reduced bacterial 16S gene copies in stool to below the limit
122 of detection (**Figure S1)**. GSEA of WT mice treated with ABX showed a significant depletion of
123 IFN-λ response genes in the ileum relative to WT mice with conventional microbiota (**Figure 1B,**
124 **1D**). These data indicate that IFN-λ response genes are present at steady-state in the ileum of
125 specific-pathogen-free mice with conventional microbiota and suggest that microbiota stimulate
126 expression of these genes in the ileum at homeostasis.

127 Type I, II, and III IFN responses have substantial gene expression overlap; therefore, to
128 prove that the IFN-λ receptor was necessary for the homeostatic expression of IFN-λ response
129 genes, we analyzed gene expression in the ileum of *Ifnlr1*$^{-/-}$ mice. Indeed, GSEA showed
130 significant reduction of IFN-λ response genes in the ileum of *Ifnlr1*$^{-/-}$ mice compared to WT mice

131 (**Figures 1B, 1E**). Furthermore, expression of IFN-λ response genes was not significantly
132 decreased in *Ifnlr1*$^{-/-}$ mice treated with ABX compared to *Ifnlr1*$^{-/-}$ mice with conventional microbiota
133 (**Figures 1B, 1F**). Together, these findings suggest that *Ifnlr1* is necessary for the bacterial
134 microbiota-dependent expression of IFN-λ response genes in the ileum at homeostasis.

135 To define a core set of bacterial microbiota-dependent, *Ifnlr1*-dependent 'homeostatic
136 ISGs', we determined the overlap of differentially expressed genes (DEGs) by defining genes
137 with: i) increased expression upon IFN-λ stimulation in WT mice, ii) decreased expression upon
138 ABX treatment in WT mice, and iii) decreased expression in *Ifnlr1*$^{-/-}$ mice relative to WT mice. The
139 DEGs shared by each of these comparisons comprised a set of 21 genes that are decreased
140 upon treatment with ABX and loss of *Ifnlr1*, and are induced in response to IFN-λ (**Figure 1G**).
141 This set of homeostatic ISGs includes antiviral genes that are dependent on bacterial microbiota
142 and the IFN-λ pathway. Hierarchical clustering of mice based on expression of these homeostatic
143 ISGs distinctly grouped mice treated with IFN-λ based on high expression of all 21 identified genes
144 (**Figure 1H**). However, clustering also separates WT mice from *Ifnlr1*$^{-/-}$ mice and ABX-treated
145 mice of both genotypes, indicating modest but significant expression of ISGs at homeostasis that
146 was lost with *Ifnlr1* deficiency or ABX treatment. Together, these analyses revealed a homeostatic
147 signature of ISGs in the ileum that depends upon the presence of bacterial microbiota and on
148 intact IFN-λ signaling.

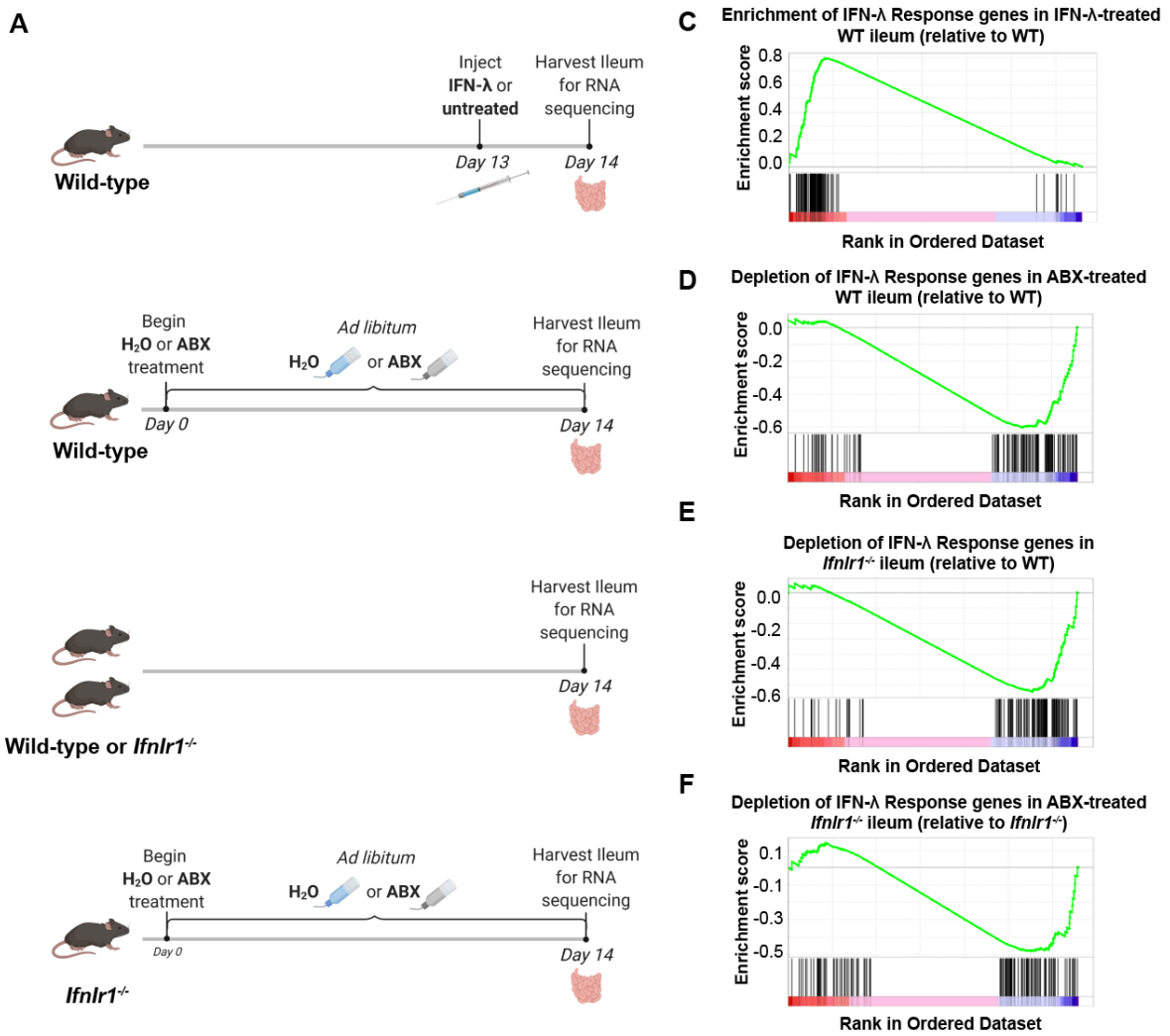

B

Comparison	Normalized Enrichment Score	False Discovery Rate q-value	Nominal p-value
IFN-λ v. untreated (WT)	1.0170078	0.0771144	< 0.0000001
ABX v. untreated (WT)	-1.0566192	0.0775862	< 0.0000001
Ifnlr1$^{-/-}$ v. WT	-1.0000759	0.0749354	< 0.0000001
ABX v. untreated (*Ifnlr1*$^{-/-}$)	-0.59921676	0.6798942	0.6798942

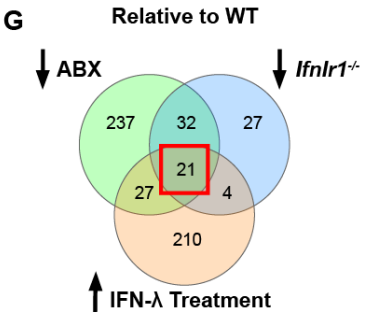

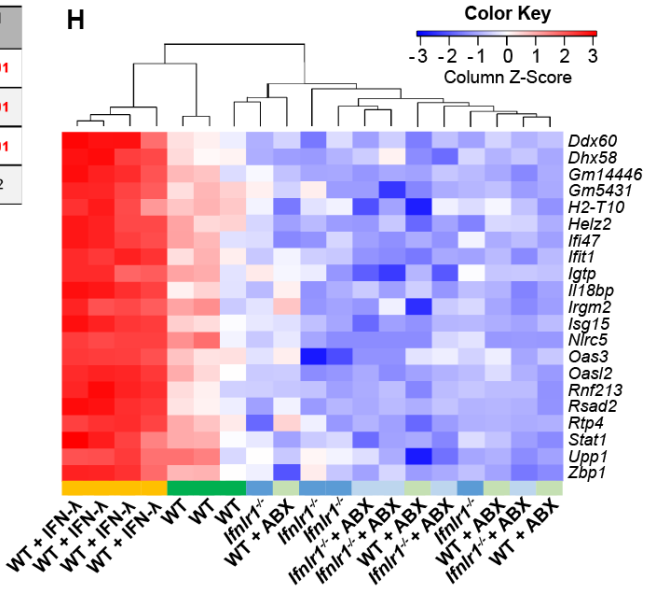

149

150 **Figure 1. Bacterial microbiota stimulate IFN-λ response genes in the ileum at homeostasis.**
151 **A.** Depiction of experimental treatments and comparison groups. Following the indicated
152 treatments, a segment of whole ileum tissue was harvested and analyzed by RNA sequencing for
153 differentially expressed genes between paired conditions. **B-E.** Gene-set enrichment analysis of
154 IFN-λ response genes was performed with the following comparisons: WT mice treated with 25μg
155 of IFN-λ relative to WT mice treated with PBS **(B)**, WT mice treated with ABX relative to untreated
156 WT mice **(C)**, *Ifnlr1*$^{-/-}$ mice relative to WT mice **(D)**, and *Ifnlr1*$^{-/-}$ mice treated with ABX relative to
157 untreated *Ifnlr1*$^{-/-}$ mice **(E)**. **F.** Statistics from gene-set enrichment analysis in **B-E** with significant
158 nominal p-values highlighted (red). **G.** A Venn diagram depicting the total number of differentially
159 expressed genes that are i) increased with IFN-λ stimulation (orange), ii) decreased with ABX
160 treatment (green), or iii) decreased in *Ifnlr1*$^{-/-}$ mice relative to WT (blue). An overlapping subset of
161 21 genes was shared among all three comparisons (red box). **H.** A heatmap with hierarchical
162 clustering of mice based on the relative expression of 21 genes that overlap in all experimental
163 groups in **G** ('homeostatic ISGs').

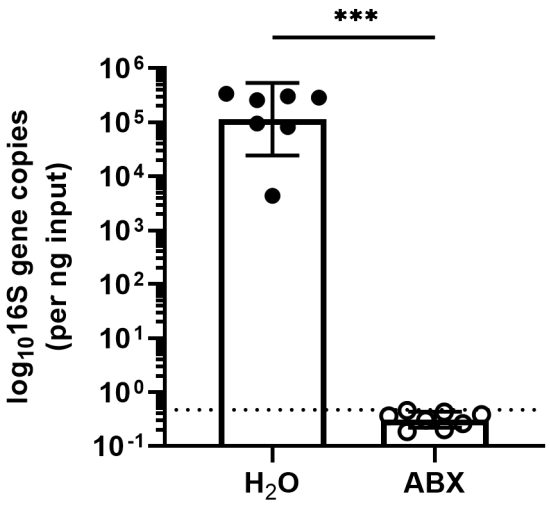

164

165 **Figure S1. Treatment with antibiotics reduces enteric 16S gene copies to below the limit of**
166 **detection.** rDNA was isolated from luminal contents of mice after 14 days of ABX-treatment. 16S

167 gene copies were assessed by qPCR and normalized to input. Limit of detection: dashed line.
168 Statistical significance was determined by Mann Whitney, where *** = $p < 0.001$.
169

170 **Homeostatic ISGs are primarily expressed in intestinal tissues**

171 To complement the results of the RNA-sequencing and extend this analysis to other tissue
172 sites**,** we quantified tissue-level expression of a panel of three ISGs by qPCR: *Ifit1, Oas1a*, and
173 *Stat1*. *Ifit1* and *Stat1* were present among the 21 homeostatic ISGs in the preceding analysis and
174 *Oas1a* was included as a representative canonical ISG that we hypothesized would be present in
175 the homeostatic signature, but did not meet the statistical criteria used to define the core set of
176 21 homeostatic ISGs (**Figure 1G and 1H**). We assessed absolute abundance of these ISG
177 transcripts in the ileum, colon, mesenteric lymph nodes (MLN), and spleen of WT and *Ifnlr1*$^{-/-}$ mice
178 with or without ABX treatment (**Figures 2A-C**). Consistent with our RNA-seq data, these ISGs
179 were reduced in the ilea of *Ifnlr1*$^{-/-}$ mice and ABX-treated WT mice compared to WT mice with
180 conventional microbiota (**Figure 2A**). Secondly, homeostatic ISGs were expressed in WT colonic
181 tissue and were significantly decreased in colonic tissue of *Ifnlr1*$^{-/-}$ mice and ABX-treated WT mice
182 (**Figure 2B**), indicating that homeostatic ISGs in both the ileum and colon were dependent on
183 *Ifnlr1* and the bacterial microbiota. To confirm that treatment with ABX does not ablate the ability
184 of the intestine to respond to IFN-λ, we stimulated WT and ABX-treated mice with intraperitoneal
185 IFN-λ and harvested ileum tissue. Stimulation with small amounts of IFN-λ rescued ISG
186 expression in whole tissue (**Figure S2**), indicating that that reduction of homeostatic ISG
187 expression upon treatment with ABX is not due to an inability for the intestinal epithelium to
188 respond to IFN-λ.

189 Enteric colonization by bacteria was shown to stimulate systemic type I IFN responses
190 (Abt et al., 2012; Bradley et al., 2019; Ganal et al., 2012; Steed et al., 2017; Stefan et al., 2020;
191 Winkler et al., 2020), so we assessed whether the decreases in ISGs upon ABX treatment or loss
192 of *Ifnlr1* in the ileum were recapitulated in systemic immune tissues. We quantified *Ifit1*, *Stat1,*

193 and *Oas1a* expression in the mesenteric lymph nodes (MLN) spleen and found that ABX
194 treatment and *Ifnlr1* deletion did not reduce ISGs in these tissues (**Figure 2C**). Although we
195 observe increases in *Ifit1* expression in MLN upon treatment with ABX, these results are not
196 recapitulated by *Stat1* and *Oas1a* expression, and no significant changes in ISG expression were
197 detected in the spleen. Cumulatively, these data indicate that homeostatic ISGs include genes
198 beyond the core signature identified in **Figure 1** (e.g. *Oas1a*), that homeostatic ISGs are present
199 in colonic tissue, and that homeostatic IFN-λ stimulated genes are most prominent in enteric
200 tissues.

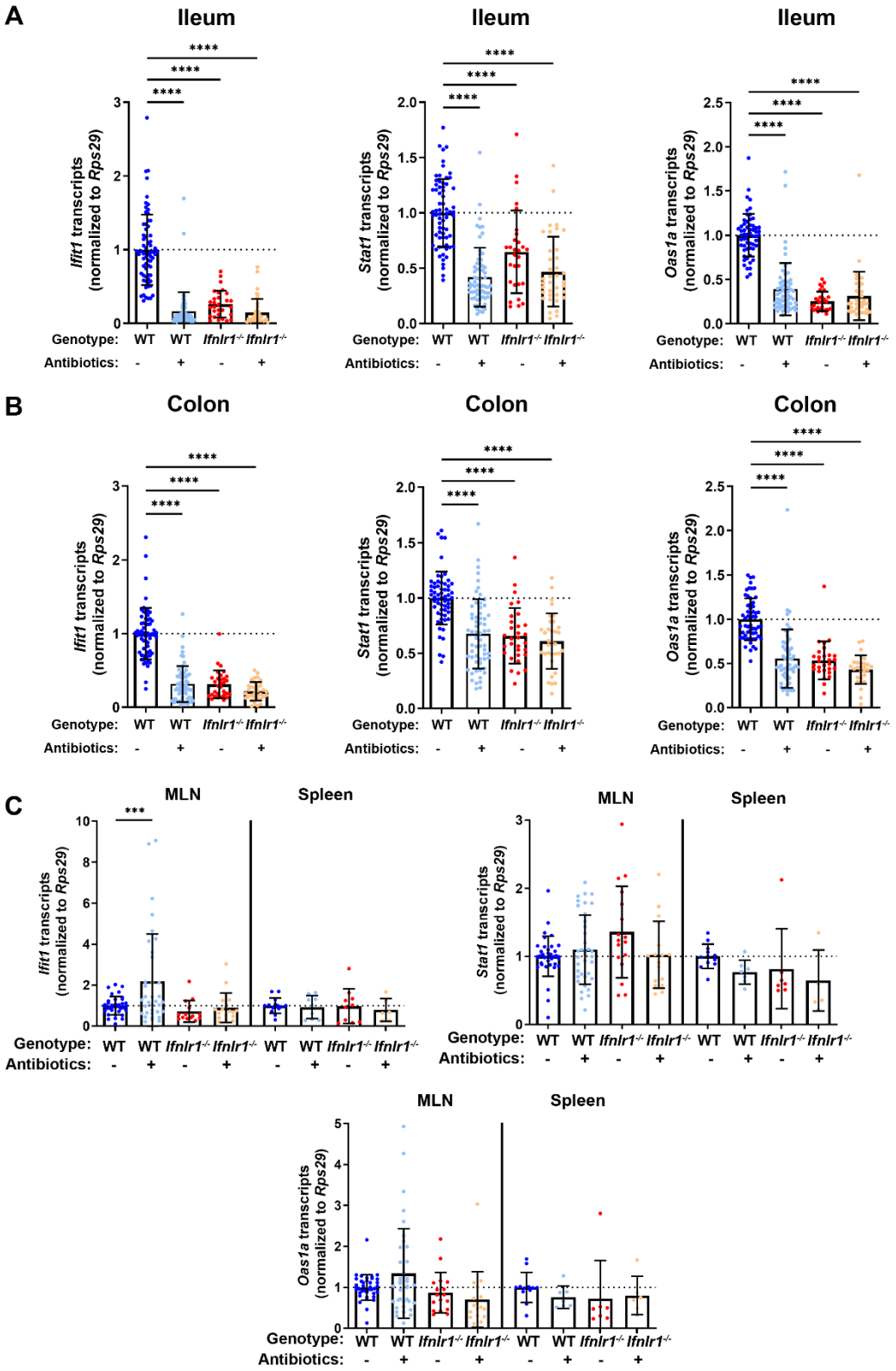

Figure 2. Homeostatic ISGs are primarily expressed in intestinal tissues. A segment of ileum or colon tissue from WT or *Ifnlr1*$^{-/-}$ mice was harvested following H_2O or ABX treatment and the

ISGs *Ifit1*, *Stat1*, and *Oas1a* were analyzed by qPCR. Transcripts were quantified in ileum **(A)**, colon **(B),** or MLN and spleen **(C)** with normalization to untreated WT mice. Data points represent individual mice. Statistical significance was determined by one-way ANOVA with Dunnett's multiple comparisons. * = p < 0.05, ** = p < 0.01, *** = p < 0.001, **** = p < 0.0001.

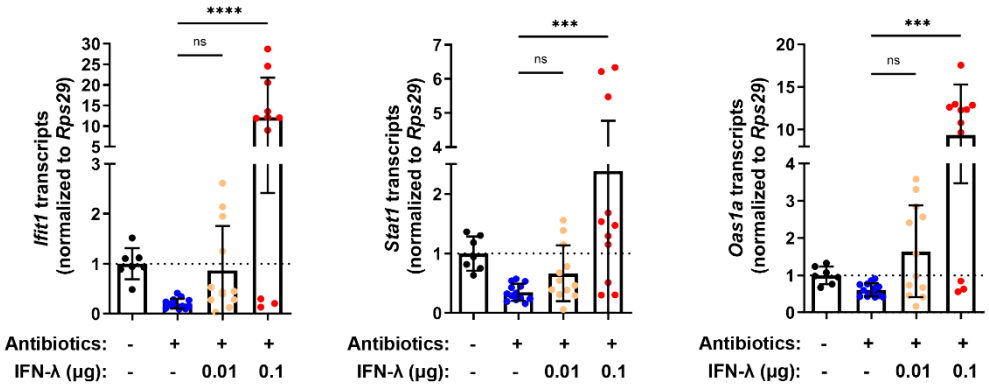

Figure S2. Treatment with antibiotics does not ablate responsiveness to IFN-λ. *Ifit1*, *Stat1*, and *Oas1a* expression was quantified in the ileum of WT mice treated with or without ABX and was normalized to untreated mice. Increasing quantities of IFN-λ were intraperitoneally injected into ABX-treated mice to rescue basal ISG expression. Statistical significance was determined by Kruskal-Wallis test with Dunn's multiple comparisons with *** = p < 0.001, and **** = p < 0.0001.

Homeostatic ISG expression in the intestine is independent of type I IFN

To determine whether detection of enteric bacteria by TLRs stimulates homeostatic ISGs, we measured tissue ISG expression in mice that were deficient in TRIF or MYD88. Signaling through TRIF results in activation of interferon regulatory factors (IRFs), such as IRF3 and IRF7, that commonly contribute to IFN induction (Honda et al., 2005a; Osterlund et al., 2007; Schmid et al., 2010). Additionally, signaling through MYD88 can aid initiation of IFN expression, through nuclear factor kappa-light-chain-enhancer of activated B cells (NF-κB) transcription factor family members (Osterlund et al., 2007) and IRF7 (Honda et al., 2005b; Tomasello et al., 2018). *Ifit1* expression in the ileum and colon of *Trif*$^{-/-}$ mice was not significantly different than in WT mice,

224 and *Ifit1* expression was reduced with ABX in *Trif*$^{-/-}$ mice (**Figure 3A**). However, we found that
225 mice lacking *Myd88* exhibited tissue-specific decreases in *Ifit1* expression, with significant
226 decreases in the ileum, but not in the colon, relative to WT mice (**Figure 3A)**. These data are
227 consistent with a previous report (Stockinger et al., 2014) and suggest that signaling through
228 MYD88, but not TRIF, is necessary for homeostatic ISG expression in the ileum, whereas other
229 factors may dominate in the colon.

230 To expand these findings, we assessed the role of IRF3 and IRF7 transcription factors
231 that are commonly activated downstream of MYD88 and TRIF. We did not observe significant
232 decreases in *Ifit1* expression in the ileum or the colon of *Irf3*$^{-/-}$ mice as compared to WT (**Figure**
233 **3B**), indicating that IRF3 is not required for homeostatic IFN-λ induction. However, we observed
234 a modest (two-fold) decrease in *Ifit1* expression in both the ileum and colon of *Irf7*$^{-/-}$ mice when
235 compared to WT mice (**Figure 3B**). Although IRF7 is implicated by these data, it does not appear
236 to be strictly required for homeostatic expression of *Ifit1* because expression is further reduced
237 by ABX treatment (**Figure 3B**). Therefore, these data suggest that IRF7 cooperates with other
238 factors in the homeostatic ISG response to the bacterial microbiota.

239 Type I and III IFNs stimulate overlapping ISG responses that are both dependent on
240 STAT1. Therefore, to further investigate the contribution of type I IFN signaling to homeostatic
241 ISG expression, we quantified *Ifit1* expression in ileum and colon tissue from *Ifnar1*$^{-/-}$ or *Stat1*$^{-/-}$
242 mice. *Ifit1* expression was not significantly different in either ileum of colon tissue of *Ifnar1*$^{-/-}$ mice
243 compared to WT (**Figure 3C**). However, *Ifit1* expression was significantly lower in ileum and colon
244 tissue of *Stat1*$^{-/-}$ mice compared to *Ifnar1*$^{-/-}$ and WT mice. Importantly, treatment of *Stat1*$^{-/-}$ mice
245 with ABX did not further reduce *Ifit1* expression, emphasizing the necessity of STAT1 for this
246 homeostatic ISG response.

247 Lastly, to determine whether type I IFN signaling plays a compensatory role in homeostatic
248 ISG expression in the absence of *Ifnlr1*, we bred mice with heterozygous expression of both *Ifnlr1*
249 and *Ifnar1* (*Ifnlr1*^{Het}/*Ifnar1*^{Het}) with mice that lack *Ifnlr1* and *Ifnar1* (*Ifnlr1*^{KO}/*Ifnar1*^{KO}). This breeding

250 scheme produced littermate-matched mice that were *Ifnlr1*^{Het}/*Ifnar1*^{Het}, *Ifnlr1*^{KO}/*Ifnar1*^{KO}, and mice
251 singly deficient in *Ifnlr1* (*Ifnlr1*^{KO}/*Ifnar1*^{Het}) or *Ifnar1* (*Ifnlr1*^{Het}/*Ifnar1*^{KO}). We found that *Ifit1*
252 expression was not significantly different in *Ifnlr1*^{Het}/*Ifnar1*^{KO} relative to *Ifnlr1*^{Het}/*Ifnar1*^{Het} controls
253 in stripped epithelium (**Figure 3D**). *Ifit1* expression in *Ifnlr1*^{KO}/*Ifnar1*^{Het} was significantly lower
254 compared to *Ifnlr1*^{Het}/*Ifnar1*^{Het} controls, but was not significantly different from *Ifnlr1*^{KO}/*Ifnar1*^{KO}
255 mice (**Figure 3D**). Cumulatively, these data indicate that homeostatic ISG expression in the
256 intestine is partly dependent on MYD88 and IRF7, and is independent of type I IFN signaling.

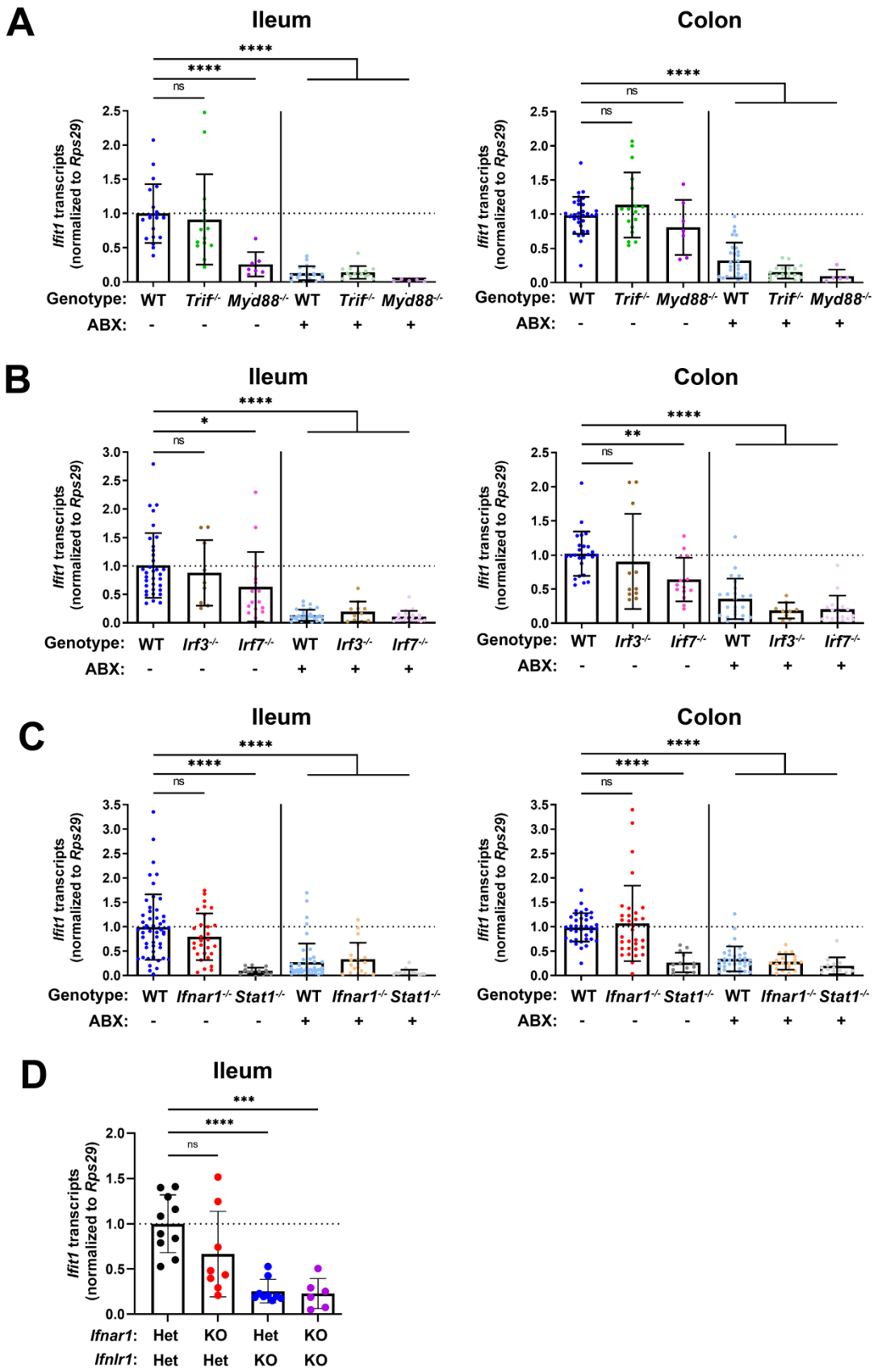
A
Ileum
Colon
****
****
ns
Ifit1 transcripts (normalized to Rps29)
Genotype: WT Trif-/- Myd88-/- WT Trif-/- Myd88-/-
ABX: - - - + + +
B
Ileum
Colon
*
**
Genotype: WT Irf3-/- Irf7-/- WT Irf3-/- Irf7-/-
C
Genotype: WT Ifnar1-/- Stat1-/- WT Ifnar1-/- Stat1-/-
D
***
Ifnar1: Het KO Het KO
Ifnlr1: Het Het KO KO

257

258 **Figure 3. Homeostatic ISG expression is independent of type I IFN.** *Ifit1* expression levels
259 were assessed by qPCR from the ileum or colon of **(A)** *Trif*$^{-/-}$ and *Myd88*$^{-/-}$, **(B)** *Irf3*$^{-/-}$ *and Irf7*$^{-/-}$, or
260 **(C)** *Ifnar1*$^{-/-}$ and *Stat1*$^{-/-}$ mice treated with or without ABX normalized to untreated, WT mice. Some
261 WT controls are shared across experiments in **(A-C). D.** *Ifit1* expression was measured by qPCR
262 in stripped epithelium of indicated genotypes. Statistical significance was determined by one-way
263 ANOVA with Dunnett's multiple comparisons in **A-D**, where * = $p < 0.05$, ** = $p < 0.01$, *** = $p <$
264 0.001, **** = $p < 0.0001$.
265

266 **Homeostatic ISG expression in the intestine is restricted to epithelial cells**

267 Given the primarily epithelial expression of *Ifnlr1*, we assessed which compartment of the
268 ileum expresses homeostatic ISGs by isolating a stripped intestinal epithelial fraction and digested
269 underlying lamina propria. We assessed ISG expression in these two fractions from WT and *Ifnlr1*$^{-}$
270 $^{/-}$ mice treated with or without ABX. Treatment with ABX or loss of *Ifnlr1* reduced homeostatic
271 ISGs in the IEC fraction, but the lamina propria had low expression of these ISGs relative to the
272 epithelium of untreated WT mice, regardless of treatment or genotype (**Figure 4A**).

273 IECs express abundant *Ifnlr1*, but other intra-epithelial cell types do not (Mahlakõiv et al.,
274 2015; Sommereyns et al., 2008). To determine whether *Ifnlr1* expression by IECs was required
275 for homeostatic ISG expression, we used mice with IECs that are conditionally deficient in *Ifnlr1*
276 (*Ifnlr1*$^{\Delta IEC}$) and littermates that retain normal *Ifnlr1* expression (*Ifnlr1*$^{flox/flox}$) (Baldridge et al., 2017).
277 *Ifit1* and *Oas1a* expression in the ileum (**Figure 4B**) and colon (**Figure 4C**) of *Ifnlr1*$^{flox/flox}$ mice was
278 decreased upon treatment with ABX, consistent with the phenotype observed in WT mice.
279 Conditional deletion of *Ifnlr1* in IECs reduced *Ifit1* and *Oas1a* to a similar extent as the reduction
280 observed in *Ifnlr1*$^{-/-}$ animals, above (**Figures 2A and 2B**). Together, these findings indicate that
281 homeostatic ISGs are dependent on *Ifnlr1*-expression by IECs.

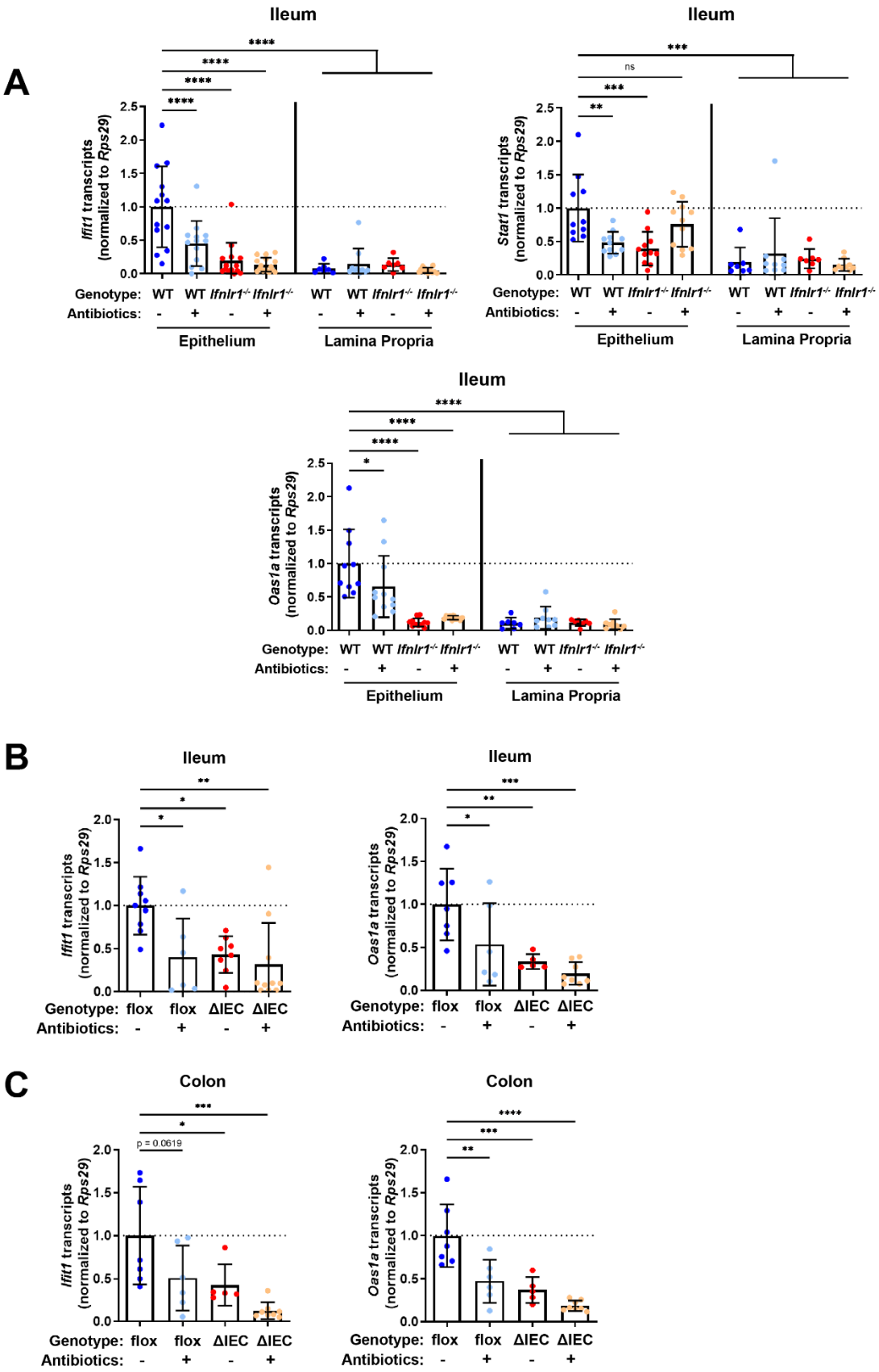
A
Ileum
Ifit1 transcripts (normalized to Rps29)
Genotype: WT WT Ifnlr1-/- Ifnlr1-/- WT WT Ifnlr1-/- Ifnlr1-/-
Antibiotics: - + - + - + - +
Epithelium
Lamina Propria
Ileum
Stat1 transcripts (normalized to Rps29)
ns
Ileum
Oas1a transcripts (normalized to Rps29)
B
Ileum
Ifit1 transcripts (normalized to Rps29)
Genotype: flox flox ΔIEC ΔIEC
Antibiotics: - + - +
Ileum
Oas1a transcripts (normalized to Rps29)
C
Colon
p = 0.0619
Colon

282

283 **Figure 4. Homeostatic ISG expression in the intestine is restricted to epithelial cells**. **A.**
284 *Ifit1*, *Stat1*, and *Oas1a* expression was quantified in rough epithelial fractions or in the lamina
285 propria digested ileum. Comparisons were performed between WT and *Ifnlr1*$^{-/-}$ mice with or
286 without ABX treatment, and ISG expression was normalized to WT values. **B and C.** *Ifit1* and
287 *Oas1a* expression from the **(B)** ileum or **(C)** colon of mice with conditional presence (flox) or
288 absence (ΔIEC) of *Ifnlr1* in intestinal epithelial cells. Statistical significance was determined by
289 one-way ANOVA with Dunnett's multiple comparisons. * = $p < 0.05$, ** = $p < 0.01$, *** = $p < 0.001$.
290

291 **Bacterial microbiota stimulate expression of *Ifnl2/3* by CD45-positive cells**

292 To determine which cellular compartment produces IFN-λ in response to bacterial
293 microbiota at homeostasis, we enriched cell subsets from epithelial or lamina propria fractions of
294 the ileum for quantification of IFN-λ transcripts (*Ifnl2/3)* by qPCR. We treated WT mice with
295 control, ABX, or stimulation with a synthetic dsRNA analogue (poly I:C) as a positive-control. We
296 then magnet-enriched EpCAM+ or CD45+ cells from stripped intestinal epithelium or digested
297 lamina propria ileal tissue (**Figure S3**). We found that CD45+ cells from the intestinal epithelial
298 and lamina propria fraction expressed detectable *Ifnl2/3* at homeostasis, but EpCAM+ cells did
299 not, which is consistent with a previous study (Mahlakõiv et al., 2015). However, in ABX-treated
300 mice, we found that expression of *Ifnl2/3* in CD45+ cells from the epithelial fraction was
301 significantly reduced, and CD45+ cells from lamina propria had a marginal ($p = 0.0523$) reduction
302 in *Ifnl2/3* expression (**Figure 5A**). Therefore, we conclude that epithelium-associated CD45+
303 leukocytes are the likely source of homeostatic IFN-λ in response to bacterial microbiota.

304 Similar to *Ifnl2/3*, we found that CD45+ cells of the epithelial fraction modestly expressed
305 *Ifnb1* at homeostasis. Additionally, CD45+ cells of the lamina propria robustly expressed *Ifnb1* at
306 homeostasis. However, unlike *Ifnl2/3*, *Ifnb1* was not decreased in mice treated with ABX (**Figure**
307 **5B**). These data indicate that *Ifnb1* expression by CD45+ cells in the intestine is less dependent

308 on stimulation by bacterial microbiota relative to *Ifnl2/3*, consistent with the dominant role of IFN-
309 λ responses in driving homeostatic ISG expression in the epithelium.

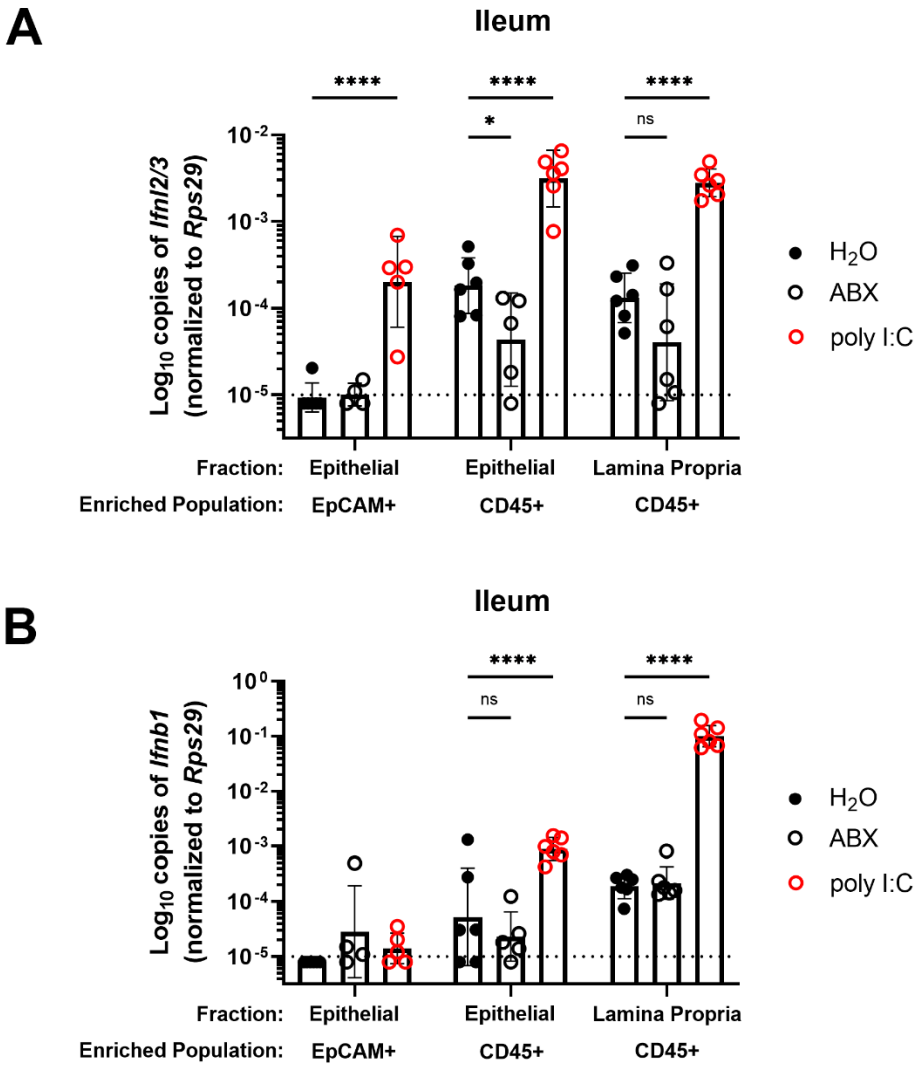

310

311 **Figure 5. Bacterial microbiota stimulate expression of *Ifnl2/3* by CD45-positive cells. A-B.**
312 The ileal epithelium and lamina propria was harvested from WT mice treated with H_2O, ABX, or
313 stimulated with poly I:C. Resulting cell suspensions were enriched for EpCAM-positive and CD45-
314 positive cells by magnetic separation. **(A)** *Ifnl2/3* expression and **(B)** *Ifnb1* expression was
315 quantified from each enriched cellular fraction by qPCR. Statistical significance was determined
316 by two-way ANOVA with Dunnett's multiple comparisons, where * = $p < 0.05$ and **** = $p < 0.0001$.

317

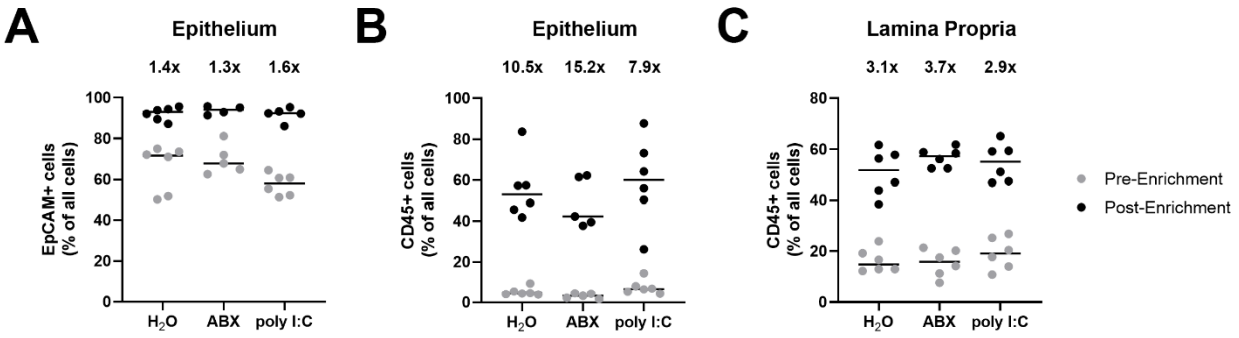

Figure S3. Enrichment of EpCAM+ and CD45+ cells from the intestinal epithelium and lamina propria. A-C. The ileal epithelium and lamina propria was harvested from WT mice treated with H_2O, ABX, or stimulated with poly I:C. Resulting cell suspensions were enriched for EpCAM-positive and CD45-positive cells and the purity of cell populations pre- and post-enrichment were quantified by flow cytometry. The percentage of cells with surface expression of **(A)** EpCAM or **(B)** CD45 prior to- and following- enrichment from stripped intestinal epithelium. **C.** The percentage of cells with surface expression of CD45 prior to and following CD45 enrichment from isolated lamina propria. Mean fold enrichment for each condition is noted above each column.

Homeostatic ISG expression in the small intestine is highly localized

Homeostatic ISG expression in the ileum was of relatively low magnitude when compared to IFN-λ treatment (**Figures 1-2**). Therefore, we hypothesized that a low abundance of homeostatic ISG expression would be uniformly distributed between IECs of the intestinal epithelium, and we sought to assess the distribution of the homeostatic ISG, *Ifit1*, using *in situ* hybridization (RNAscope) (**Figures 6A-G**). Contrary to our hypothesis, RNAscope staining of the ileum from untreated WT mice revealed localized pockets of robust *Ifit1* expression rather than ubiquitously low expression (**Figure 6A**). Additionally, *Ifit1* localization was skewed away from the crypt and towards the tips of individual villi within the ileum, and this localization was not specific to *Ifit1* because the distinct ISG *Usp18* was colocalized with *Ifit1* (**Figure 6A**). These data indicate

339 that homeostatic ISGs are co-expressed primarily in mature enterocytes that are most distally
340 located in villi. We determined that localized ISG expression was not due to a localized capacity
341 for IEC IFN-λ response because stimulation with exogenous IFN-λ resulted in *Ifit1* expression
342 throughout the entire intestinal epithelium (**Figure S4**). Additionally, the non-uniform distribution
343 of homeostatic *Ifit1* expression was ablated in the ileum of mice treated with ABX (**Figures 6B-**
344 **D**), consistent with a dependency on bacterial microbiota. To determine whether localized *Ifit1*
345 expression was dependent on IEC expression of *Ifnlr1*, we assessed the distribution of *Ifit1*
346 expression in the ilea of littermate *Ifnlr1*$^{flox/flox}$ and *Ifnlr1*$^{\Delta IEC}$ mice. We found that the localized *Ifit1*
347 expression observed in untreated WT mice was recapitulated in *Ifnlr1*$^{flox/flox}$ mice (**Figure 6E**), but
348 these areas of ISG expression were ablated in *Ifnlr1*$^{\Delta IEC}$ mice (**Figures 6F and 6G**). Lastly, we
349 found that this discrete localization of the homeostatic ISG response is not limited to the ileum,
350 as localized *Ifit1* staining is also observed in the colonic epithelium (**Figure S5**). Together, our
351 analyses indicated that homeostatic ISGs are expressed in a highly localized manner within the
352 intestinal epithelium.

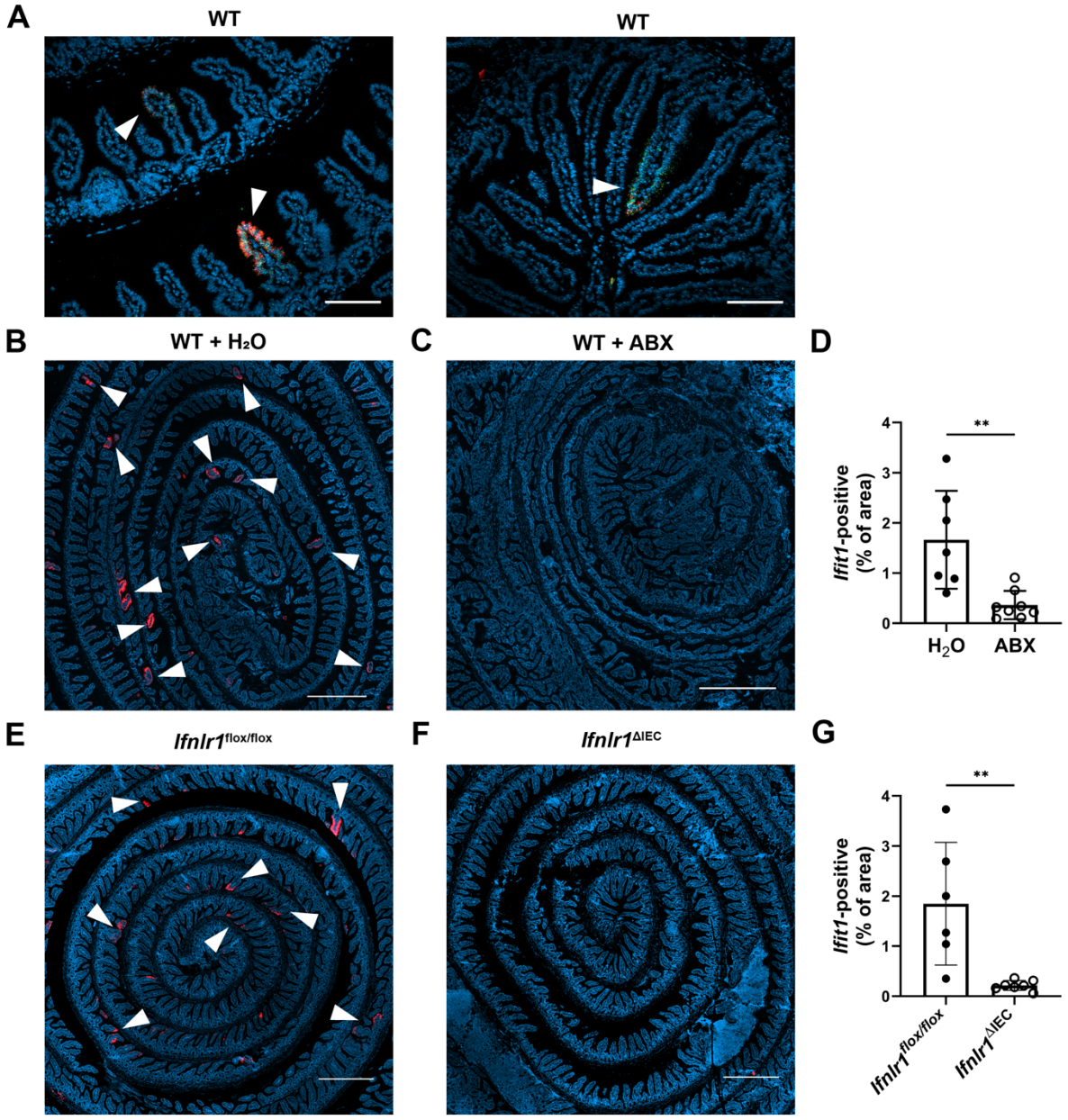

353

354 **Figure 6. Homeostatic ISG expression in the small intestine is highly localized**. The ilea of
355 WT, *Ifnlr1*$^{flox/flox}$, or *Ifnlr1*$^{\Delta IEC}$ mice were harvested, processed into a Swiss rolls, and stained by *in*
356 *situ* hybridization for the ISGs, *Ifit1* (red) and *Usp18* (green), with a DAPI (blue) counterstain. **A.**
357 Representative high-magnification images of co-localized *Ifit1* (red) and *Usp18* (green)
358 expression in the ileum of WT mice, see arrows. **B-D.** WT mice treated with H_2O control or ABX
359 with quantification of *Ifit1* area relative to the total area of the section across replicate mice. **E-G.**
360 *Ifnlr1*$^{flox/flox}$ or *Ifnlr1*$^{\Delta IEC}$ mice at homeostasis with quantification of *Ifit1* area relative to the total area

of the section across replicate mice. Scale bar = 100μm in **A** and 500μm in **B-G** and. Statistical significance was calculated by unpaired t-test where ** = p < 0.01. Each data point in **D** and **G** represents an individual mouse from 2 replicate experiments, with n = 7-8 for each condition.

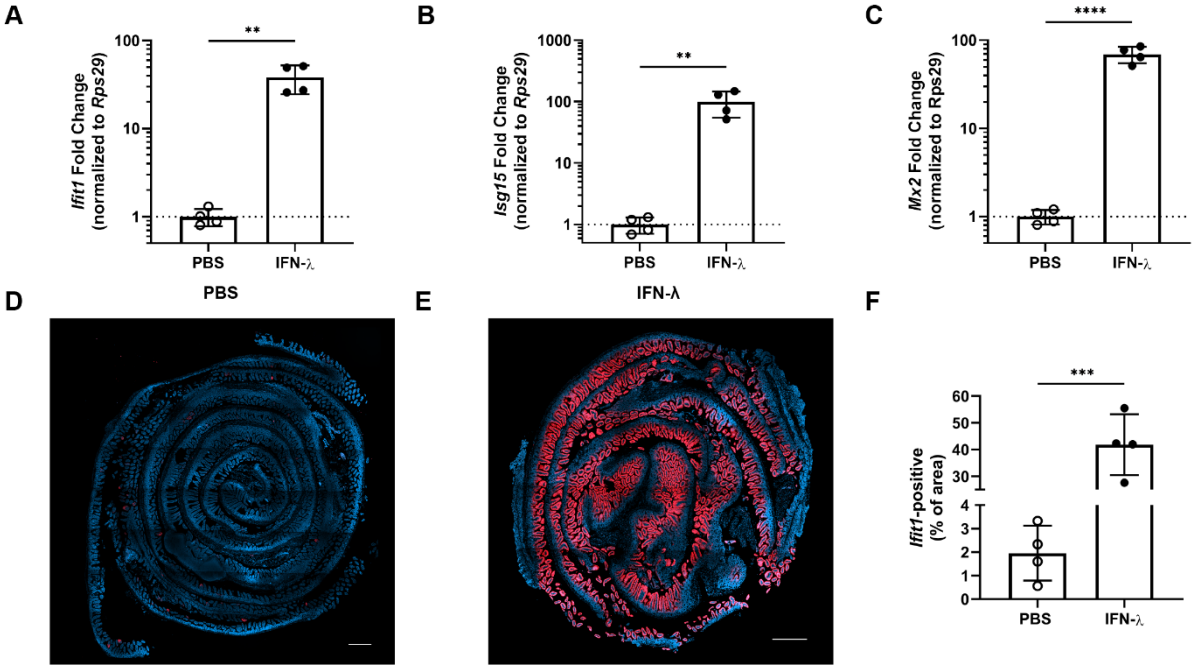

Figure S4. The entire intestinal epithelium is responsive to IFN-λ. Wild-type mice were injected with PBS or 3μg of pegylated IFN-λ3. The ileum was harvested after four hours and a small section was assessed for expression of the ISGs: *Ifit1* **(A)**, *Isg15* **(B)**, and *Mx2* **(C)** by qPCR. The remaining tissue was stained by RNAscope for the ISG, *Ifit1* (red), with a DAPI (blue) counterstain. **D-E.** Representative images from the ileum of mice injected with PBS **(D)** or IFN-λ **(E). F.** Quantification of *Ifit1* area relative to the total area of the section across replicate mice. Scale bar = 500μm. Statistical significance was determined by unpaired t-test with ** = p < 0.01, *** = p < 0.001, and **** = p < 0.0001.

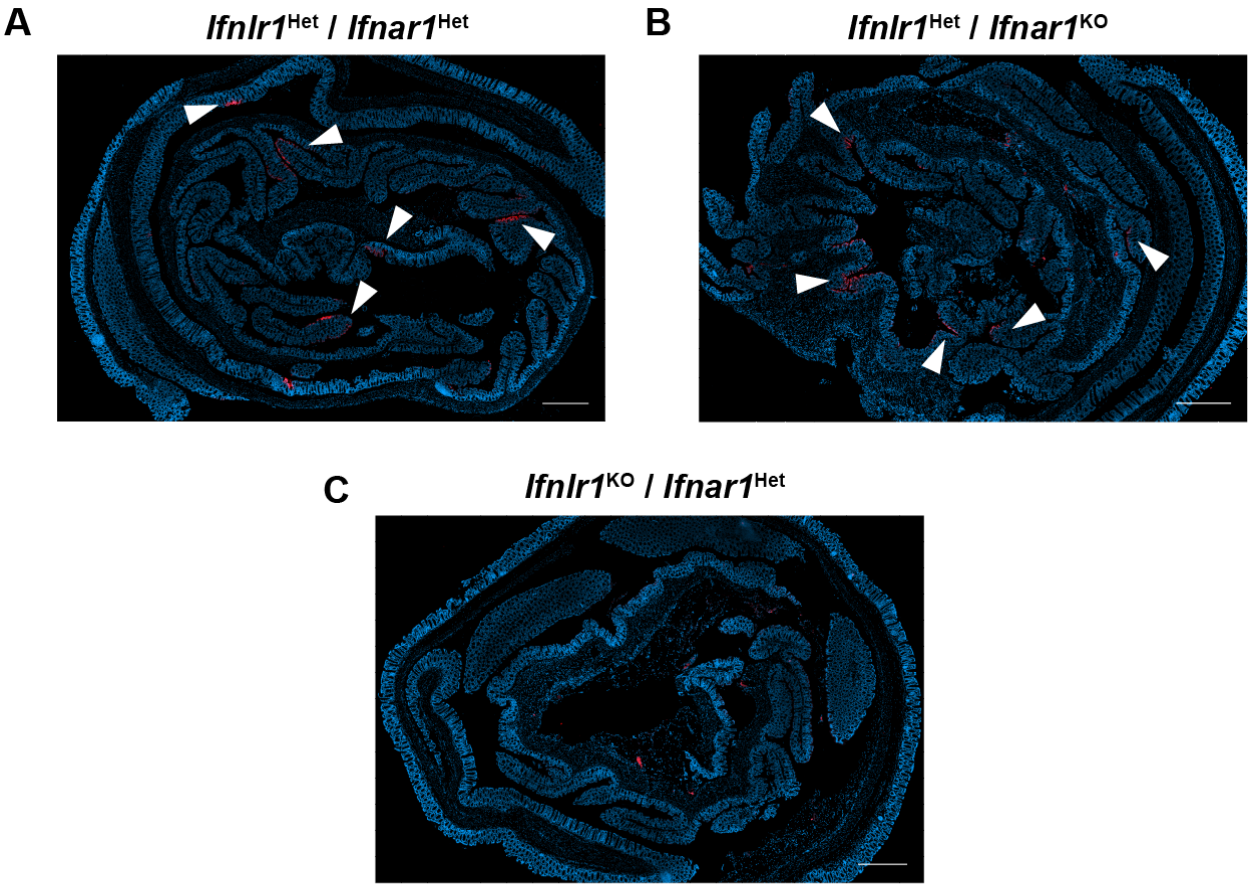

374

375 **Figure S5. Homeostatic ISG expression is also highly localized in the colon.** The colon of
376 *Ifnlr1*^{Het}/*Ifnar1*^{Het}, *Ifnlr1*^{Het}/*Ifnar1*^{KO}, and *Ifnlr1*^{KO}/*Ifnar1*^{Het} mice was harvested and stained by
377 RNAscope for the ISG, *Ifit1* (red), with a DAPI (blue) counterstain. Representative images from
378 *Ifnlr1*^{Het}/*Ifnar1*^{Het} **(A),** *Ifnlr1*^{Het}/*Ifnar1*^{KO} **(B)**, and *Ifnlr1*^{KO}/*Ifnar1*^{Het} **(C)** mice. Scale bar = 500μm.

379

380 **Mature enterocytes express homeostatic ISGs in public single-cell datasets from mouse**
381 **and human**

382 To determine the extent of conservation for homeostatic ISG expression by IECs, we
383 performed orthogonal analyses of publicly available single-cell RNA-seq (scRNA-seq) datasets
384 from mouse (Haber et al., 2017) and human (Elmentaite et al., 2020) IECs. Recently, Haber et al.

385 published a large single-cell RNA sequencing dataset that profiled sorted IECs from the small
386 intestine of specific-pathogen-free mice and defined 15 distinct IEC subtypes (Haber et al., 2017).
387 We analyzed IECs from this dataset, and found that of the 21 homeostatic ISGs identified in
388 **Figure 1D**, 19 were present in the Haber et al. single-cell dataset. We determined the percentage
389 of each epithelial cell subtype that expresses each individual homeostatic ISG, and generated a
390 heatmap with hierarchical clustering to group IEC subtypes that have similar ISG expression
391 patterns (**Figure 7A**). Homeostatic ISGs were predominantly expressed in mature enterocyte
392 subtypes, which clustered separately from crypt-resident progenitor IECs such as transit
393 amplifying (TA) cells and stem cells (**Figure 7A**). To compare homeostatic ISG expression
394 between polar extremes of the crypt-villus axis, we grouped IEC subtypes that represented
395 enterocytes (mature enterocyte cells) and crypt cells (TA cells and stem cells) and compared the
396 overall proportions of these cells with homeostatic ISG expression. We found that a significantly
397 higher percentage of enterocytes express homeostatic ISGs than crypt cells, but that these
398 homeostatic ISGs were expressed in a relatively small proportion of enterocytes (< 20%) (**Figure**
399 **7B**). Notably, *Ifit1* (highlighted in red) was present in ~5% of enterocytes by scRNA-seq, which is
400 consistent with our observation of 1-4% *Ifit1*-positive area by imaging the mouse small intestine
401 (**Figures 6B-G**). Furthermore, the relative absence of ISG-positive crypt cells in scRNA-seq data
402 is consistent with our observation that crypt cells lacked *Ifit1* and *Usp18* expression by imaging.
403 We expanded our investigation to a scRNA-seq dataset from the ileum of healthy, human,
404 pediatric patients that was previously described (Elmentaite et al., 2020). IECs from this dataset
405 were previously clustered into eight subtypes. For our analysis of homeostatic ISG expression,
406 we excluded IEC sub-types with fewer than 20 constituent cells, which retained five subtypes:
407 enterocytes, early enterocytes, goblet cells, TA cells, and crypt. Of the 21 homeostatic ISGs
408 identified in **Figure 1D**, 14 homologous human genes were present in these data. Similar to
409 analysis in **Figure 7A,** we determined the percentage of each cell type that expresses each
410 individual homeostatic ISG and generated a heatmap of these data with hierarchical clustering to

411 group IEC subtypes that have similar ISG expression patterns (**Figure 7C**). Enterocyte, early
412 enterocyte, and goblet subtypes clustered separately from TA and crypt cells, with the highest
413 proportion of homeostatic ISGs being present in the enterocyte subtype (**Figure 7C**). As with
414 mouse IEC data, above, we grouped cell subtypes that localize in the crypt (TA cells and crypt
415 cells) and compared overall proportions of homeostatic ISG expression with the mature
416 enterocyte subtype (**Figure 7D**). Similar to mice, homeostatic ISGs were present in significantly
417 more enterocytes than crypt cells, and most homeostatic ISGs in this human dataset were present
418 in a relatively small proportion of cells (< 20%). These data suggest that ISGs are present in a
419 small proportion of IECs from healthy, human ileal tissue at homeostasis and may share the
420 localization observed in our murine analyses. Together, our analyses of these public scRNA-seq
421 datasets support our observations that homeostatic ISGs are not ubiquitously expressed
422 throughout the intestinal epithelium; rather, they are expressed in a minority of IECs and skewed
423 towards mature enterocytes along the crypt-villus axis.

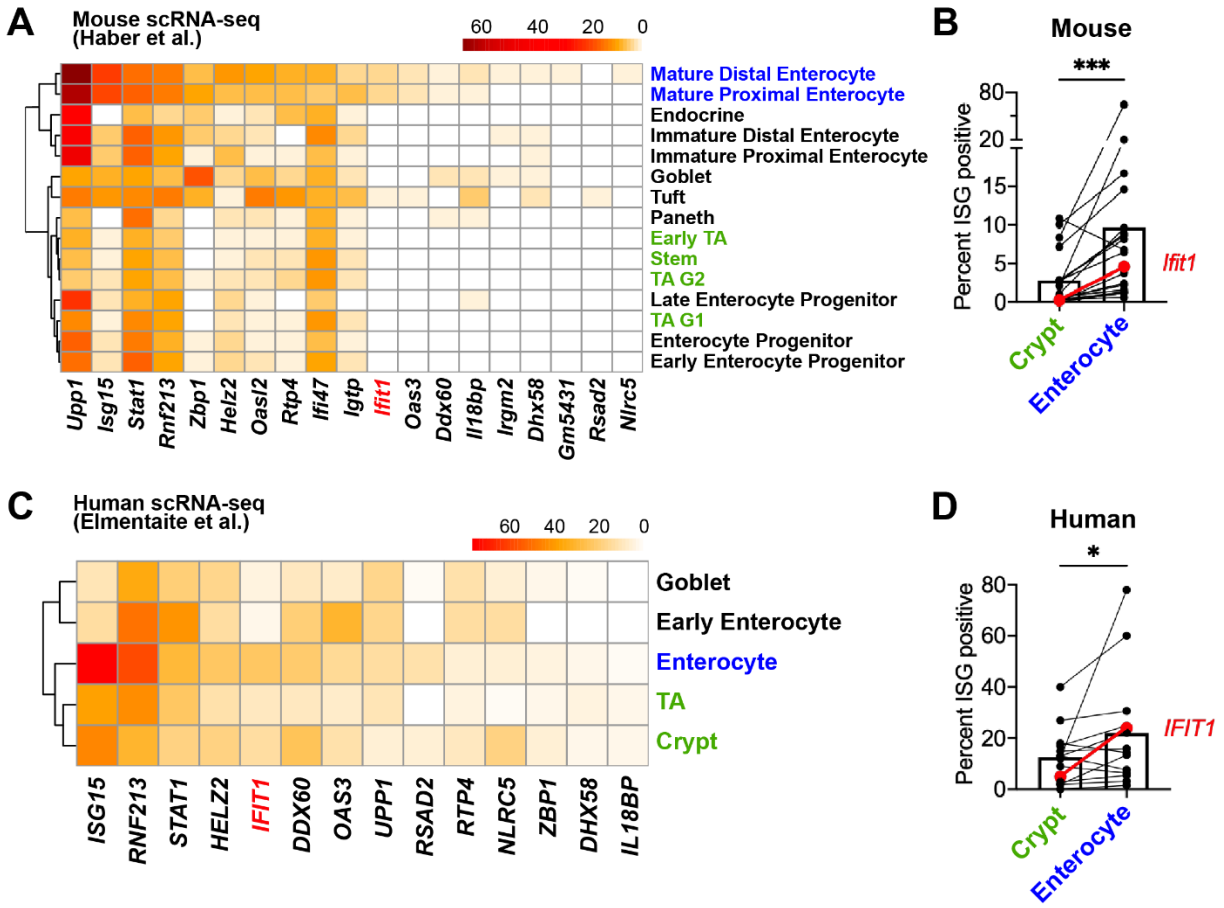

Figure 7. Mature enterocytes express homeostatic ISGs in public single-cell datasets from mouse and human. A-B. A mouse IEC single-cell transcriptional dataset (Haber et al., 2017) (GSE92332) was analyzed to determine the percentage of each epithelial cell subtypes that express homeostatic ISGs. **A.** Heatmap depicting the proportion of each epithelial cell type expressing nineteen of the twenty-one homeostatic ISGs identified in **Figure 1**. **B.** Enterocyte subtypes (blue text) and crypt-resident progenitor subtypes (green text) cells were grouped and the percentage of cells that express each homeostatic ISG was compared. **C-D.** A human IEC single-cell transcriptional dataset (Elmentaite et al., 2020) (E-MTAB-8901) was analyzed for the percentage of epithelial cell subtypes that express homeostatic ISGs. **C.** A heatmap depicting the percentage of IEC subtypes that express human orthologs of murine homeostatic ISGs identified in **Figure 1**. **D.** The mature enterocyte subtype (blue text) and crypt-resident progenitor subtypes

436 (green text) were grouped and the percentage of cells that express each homeostatic ISG was
437 compared. Lines in **B** and **D** link paired ISGs in each IEC subset. Statistical significance in **B** and
438 **D** was calculated by Wilcoxon test where * = $p < 0.05$, and *** = $p < 0.001$.
439

440 **Homeostatic ISG expression is partially restored by peroral LPS in ABX-treated mice**

441 To further define the relationship between bacteria and homeostatic ISGs, we assessed
442 whether oral administration of fecal contents or purified LPS (a bacterial MAMP and TLR4 agonist)
443 could restore localized ISG expression in mice with depleted bacterial microbiota. Control groups
444 of *Ifnlr1*$^{flox/flox}$ mice with conventional microbiota (**Figure 8A**) retained a localized *Ifit1* expression
445 pattern, whereas ABX-treated *Ifnlr1*$^{flox/flox}$ mice (**Figure 8B**) and *Ifnlr1*$^{\Delta IEC}$ mice (**Figure 8C**) lacked
446 *Ifit1* expression. Oral LPS administered to conventional *Ifnlr1*$^{flox/flox}$ mice did not significantly alter
447 the distribution or frequency of localized *Ifit1* expression (**Figure 8D**). However, localized *Ifit1*
448 expression was restored in a subset of ABX-treated *Ifnlr1*$^{flox/flox}$ mice administered LPS (**Figure**
449 **8E**). Fecal transplant of conventional microbes to ABX-treated *Ifnlr1*$^{flox/flox}$ mice was similarly
450 capable of restoring localized expression of *Ifit1* in a subset of mice (**Figure 8F**). Importantly, we
451 did not observe restoration of localized *Ifit1* expression in *Ifnlr1*$^{\Delta IEC}$ mice following LPS
452 administration (**Figure 8G**), indicating that restoration depends on IEC expression of *Ifnlr1*.

453 We noted that restoration of localized *Ifit1* signal following LPS administration or fecal
454 transplant appeared largely binary (i.e. present or absent) in our imaging data (**Figures 8E and**
455 **8F**, representative *Ifit1*-positive and *Ifit1*-negative images). Using quantification of *Ifit1* area
456 (**Figure 8H**), we stratified mice into *Ifit1*-postive and *Ifit1*-negative groups (**Figure 8I-J**) based on
457 a cut-off set at the maximal *Ifit1* area value of *Ifnlr1*$^{\Delta IEC}$ mice (dashed line in **Figure 8H**). This
458 analysis indicated 8/8 conventional *Ifnlr1*$^{flox/flox}$ mice, 0/8 ABX-treated control mice, 4/12 LPS-
459 treated mice, and 4/8 fecal transplant mice were *Ifit1*-positive (**Figure 8I-J**). Statistical analysis by
460 Fisher's exact test indicated that LPS administration modestly increased ($p = 0.1022$) the
461 proportion of mice that were *Ifit1*-positive, whereas fecal reconstitution of ABX-treated mice

462 significantly increased ($p < 0.05$) the likelihood of these mice being *Ifit1*-positive (**Figure 8J**).
463 Importantly, mice that received fecal transplant had full restoration of 16S gene copies (**Figure**
464 **8K**) despite having partial restoration of homeostatic ISGs (4/8). These findings indicate that
465 reconstitution of homeostatic ISG signal has incomplete penetrance, underscoring the partial
466 restoration by LPS administration to ABX-treated mice.

467 To corroborate these findings, we performed orthogonal analyses of *Ifit1*, *Stat1*, and
468 *Oas1a* expression in ileum tissue of WT mice treated with ABX followed by fecal transplant, LPS
469 administration, or administration of TLR9 agonist, CpG DNA (**Figure S6**). These data exhibited
470 high variance, but were consistent with imaging data in **Figure 8**, indicating a partial restoration
471 of homeostatic ISGs in 20-50% of ABX-treated mice by LPS or fecal transplant, but not CpG DNA
472 (**Figure S6**). Together, these data indicate that LPS is sufficient for localized, homeostatic ISG
473 expression to a similar extent as total microbiota, suggesting that localized exposure to bacterial
474 MAMPs is the basis for localized, homeostatic ISG expression.

475

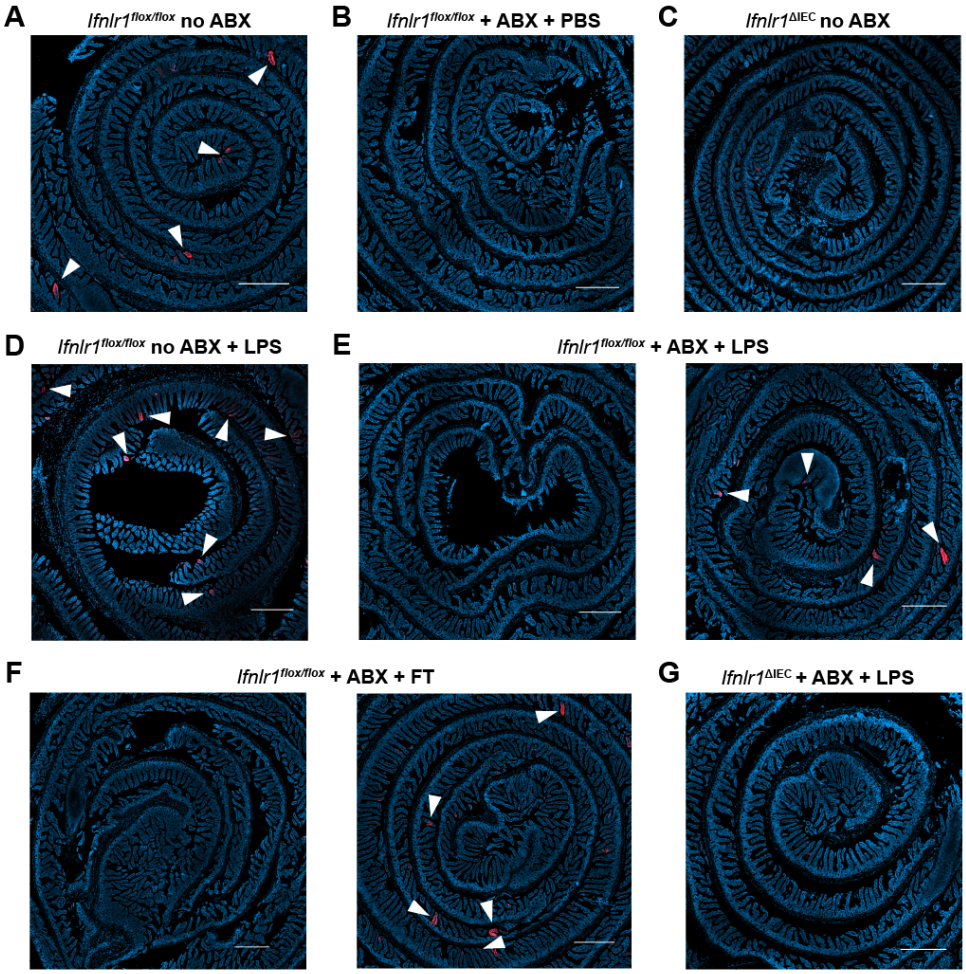

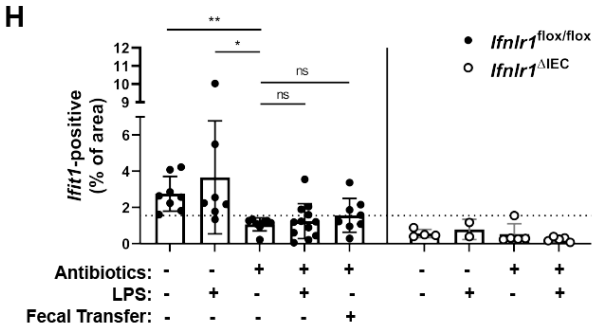

I

ABX	-	-	+	+	+
LPS	-	+	-	+	-
Fecal Transfer	-	-	-	-	+
Ifit1-positive mice / total	8/8	6/7	0/8	4/12	4/8

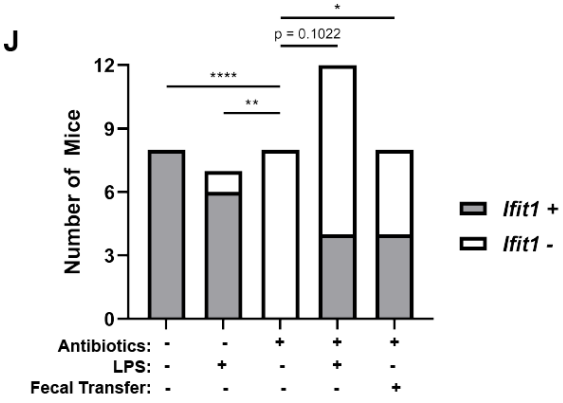

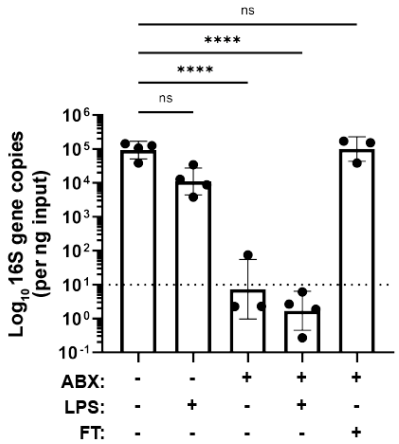

476 **Figure 8. Homeostatic ISG expression is partially restored by peroral LPS in ABX-treated**
477 **mice.** The ilea of treated WT, *Ifnlr1*$^{flox/flox}$, and *Ifnlr1*$^{\Delta IEC}$ mice were harvested, processed into Swiss
478 rolls, and stained by *in situ* hybridization for the ISG, *Ifit1* (red), with a DAPI (blue) counterstain**.**
479 **A-C.** Representative images from *Ifnlr1*$^{flox/flox}$ mice treated with H_2O control followed by PBS
480 stimulation **(A)**, ABX followed by PBS stimulation **(B)**, or from *Ifnlr1*$^{\Delta IEC}$ mice **(B)**. **D.**
481 Representative images of *Ifnlr1*$^{flox/flox}$ mice treated with H_2O control followed by LPS stimulation.
482 **E-F.** Two representative images of *Ifnlr1*$^{flox/flox}$ mice treated with ABX followed by LPS stimulation
483 **(E)** or ABX followed by fecal transplantation **(F)**. **H.** Quantification of *Ifit1* area relative to the total
484 area of each tissue section with a dashed line at the highest *Ifnlr1*$^{\Delta IEC}$ value. The proportion of
485 *Ifit1*-positive mice (above dashed line) and *Ifit1*-negative mice (below dashed line) are tabulated
486 **(I)** and graphed **(J)** for *Ifnlr1*$^{flox/flox}$ mice of each condition. **K.** rDNA was isolated from the luminal
487 contents of mice at endpoint harvest. 16S gene copies were assessed by qPCR and normalized
488 to input. Limit of detection: dashed line. Where depicted, scale bar = 500μm. Statistical
489 significance was determined by one-way ANOVA with Dunnett's multiple comparisons **(H, K)** and
490 by Fisher's exact test **(J)** where * = $p < 0.05$, ** = $p < 0.01$, and **** = $p < 0.0001$.

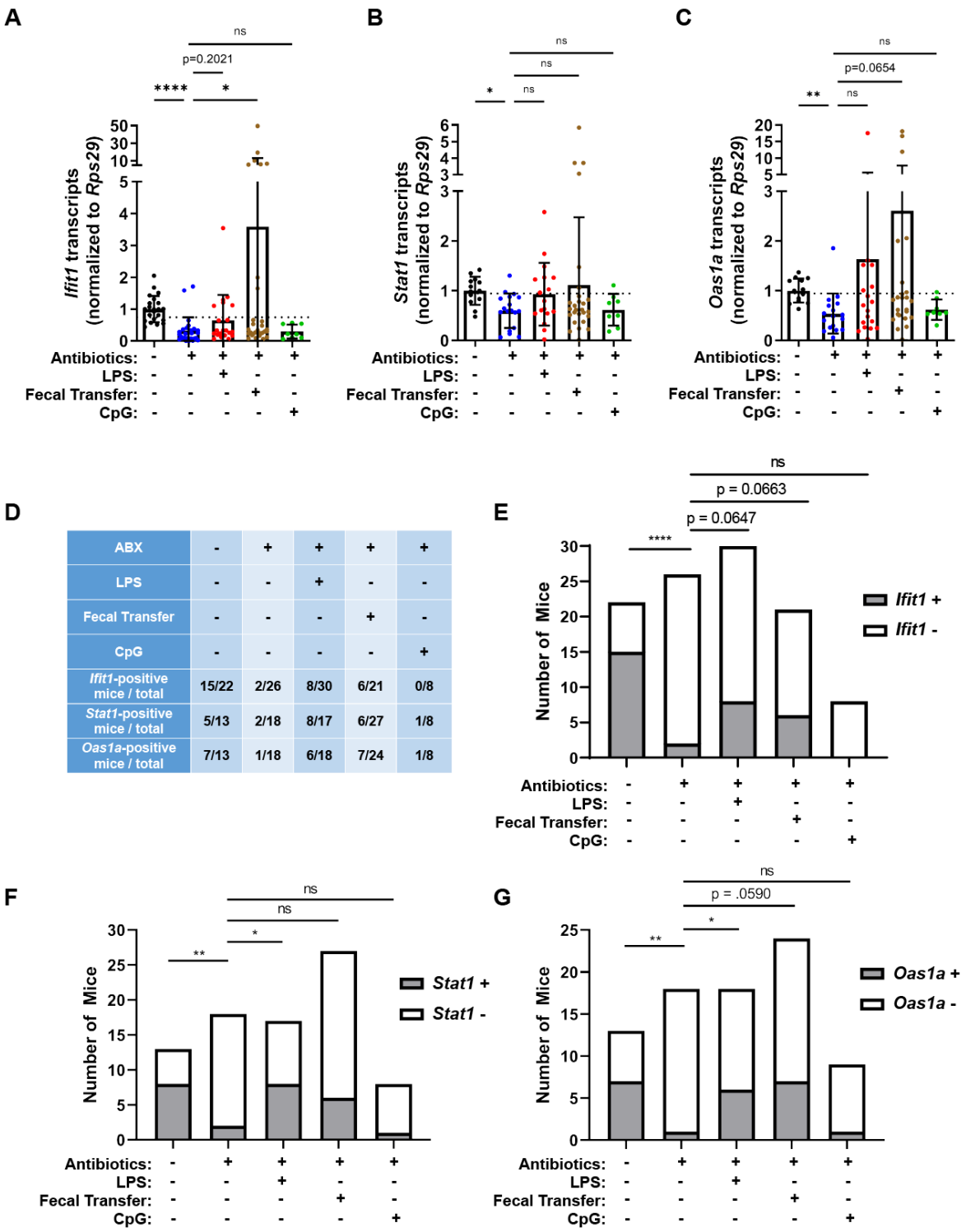

ABX	-	+	+	+	+
LPS	-	-	+	-	-
Fecal Transfer	-	-	-	+	-
CpG	-	-	-	-	+
Ifit1-positive mice / total	15/22	2/26	8/30	6/21	0/8
Stat1-positive mice / total	5/13	2/18	8/17	6/27	1/8
Oas1a-positive mice / total	7/13	1/18	6/18	7/24	1/8

Figure S6. Homeostatic ISG expression is partially restored by peroral LPS in ABX-treated mice. The ileum of treated WT, *Ifnlr1*$^{flox/flox}$, and *Ifnlr1*$^{\Delta IEC}$ mice was harvested and *Ifit1* **(A)**, *Stat1* **(B)**, and *Oas1a* **(C)** was quantified by qPCR. Delineation of positive ISG expression was

495 conservatively selected as one standard deviation above the mean of ABX-treated mice (dashed
496 line). Mice were binned into ISG-positive (above dashed line) or ISG-negative (below dashed line)
497 groups and are tabulated for each condition in **D**. The proportion of mice with expression of *Ifit1*
498 **(E)**, *Stat1* **(F)**, and *Oas1a* **(G)** are graphed for each condition. Statistical significance was
499 determine by one-way ANOVA with Dunnett's multiple comparisons **(A-C)** and by Fisher's exact
500 test **(E-G)** where * = $p < 0.05$, ** = $p < 0.01$, and **** = $p < 0.0001$.
501

502 **The homeostatic IFN-λ response preemptively protects IECs from murine rotavirus**
503 **infection**

504 To assess the capacity of homeostatic ISGs to protect IECs from viral infection, we utilized
505 infection with murine rotavirus (mRV), an IEC-tropic pathogen. Prior studies of rotaviruses have
506 identified viral immune evasion genes that block IFN induction through multiple mechanisms
507 (Arnold et al., 2013). However, we reasoned that pre-existing ISG expression stimulated by the
508 bacterial microbiome at homeostasis may preemptively protect IECs from the infection before
509 viral gene expression is initiated. To determine the role of an epithelial IFN-λ response over the
510 course of mRV infection in adult mice, we monitored daily shedding of viral genomes in the stool
511 of *Ifnlr1*$^{flox/flox}$ mice and *Ifnlr1*$^{\Delta IEC}$ littermates. We first detected mRV shedding in the stool on day
512 two after inoculation, and at this early timepoint, *Ifnlr1*$^{\Delta IEC}$ shed 20-fold more mRV genomes into
513 their stool than *Ifnlr1*$^{flox/flox}$ mice (**Figure 9A**). However, at the peak of viral shedding between days
514 three and five, there were no significant differences between *Ifnlr1*$^{flox/flox}$ and *Ifnlr1*$^{\Delta IEC}$ littermates
515 (**Figure 9A**). This similarity at peak of viral shedding was consistent with an ability of mRV to
516 evade the host IFN response once infection is established. Together, these findings suggest that
517 *Ifnlr1*$^{\Delta IEC}$ mice have defects in protection against initiation of mRV infection and that the protective
518 capacity of endogenous IFN-λ signaling against mRV is primarily prophylactic in nature.

519 To more stringently assess the capacity of *Ifnlr1* to protect IECs against the earliest stages
520 of mRV infection, we inoculated mice with 5000 SD50 (50% shedding dose) of mRV to maximize

521 the likelihood of uniform viral exposure throughout the intestine. At 12 and 24 hours post-
522 inoculation, we quantified mRV genomes in the ileum and the proportion of infected IECs (live,
523 EpCAM-positive, CD45-negative, and mRV-positive) by flow cytometry. At 24 hours post-
524 inoculation, we found that *Ifnlr1*$^{\Delta IEC}$ mice had 20-fold more mRV genomes than *Ifnlr1*$^{flox/flox}$ mice
525 (**Figure 9B**). In addition, we found that a three-fold greater proportion of IECs were infected with
526 mRV in *Ifnlr1*$^{\Delta IEC}$ mice than *Ifnlr1*$^{flox/flox}$ mice at 24 hours post-infection (**Figures 9C-F**). However,
527 the median fluorescence intensity (MFI) of mRV antigen was equivalent in mRV-infected IECs
528 from *Ifnlr1*$^{flox/flox}$ and *Ifnlr1*$^{\Delta IEC}$ mice (**Figure 9G**) and the MFI of mRV did not correlate ($r^2 = 0.0003$)
529 with the percentage of infected IECs (**Figure 9H**). This equivalent mRV antigen burden in infected
530 cells from *Ifnlr1*$^{flox/flox}$ and *Ifnlr1*$^{\Delta IEC}$ mice in combination with the lack of correlation between antigen
531 burden and percentage of infected cells suggests that the protective role of *Ifnlr1* is to prevent
532 infection of IECs rather than to limit replication within IECs after they are infected. Similar trends
533 toward an increased proportion of IEC infection in *Ifnlr1*$^{\Delta IEC}$ relative to *Ifnlr1*$^{flox/flox}$ littermates were
534 observed at 12 hours post-inoculation, but the extent of infection was 10-100 fold lower and near
535 the limit of detection (**Figure S7**). Thus 12- and 24-hour timepoints capture the earliest detectable
536 infection of IECs by mRV. Together these data indicate that *Ifnlr1* expression by IECs reduces
537 the proportion of cells initially infected by mRV, but does not limit the extent of replication once
538 infection is established, consistent with an early protective role for homeostatic ISG expression
539 that preempts viral IFN evasion mechanisms.

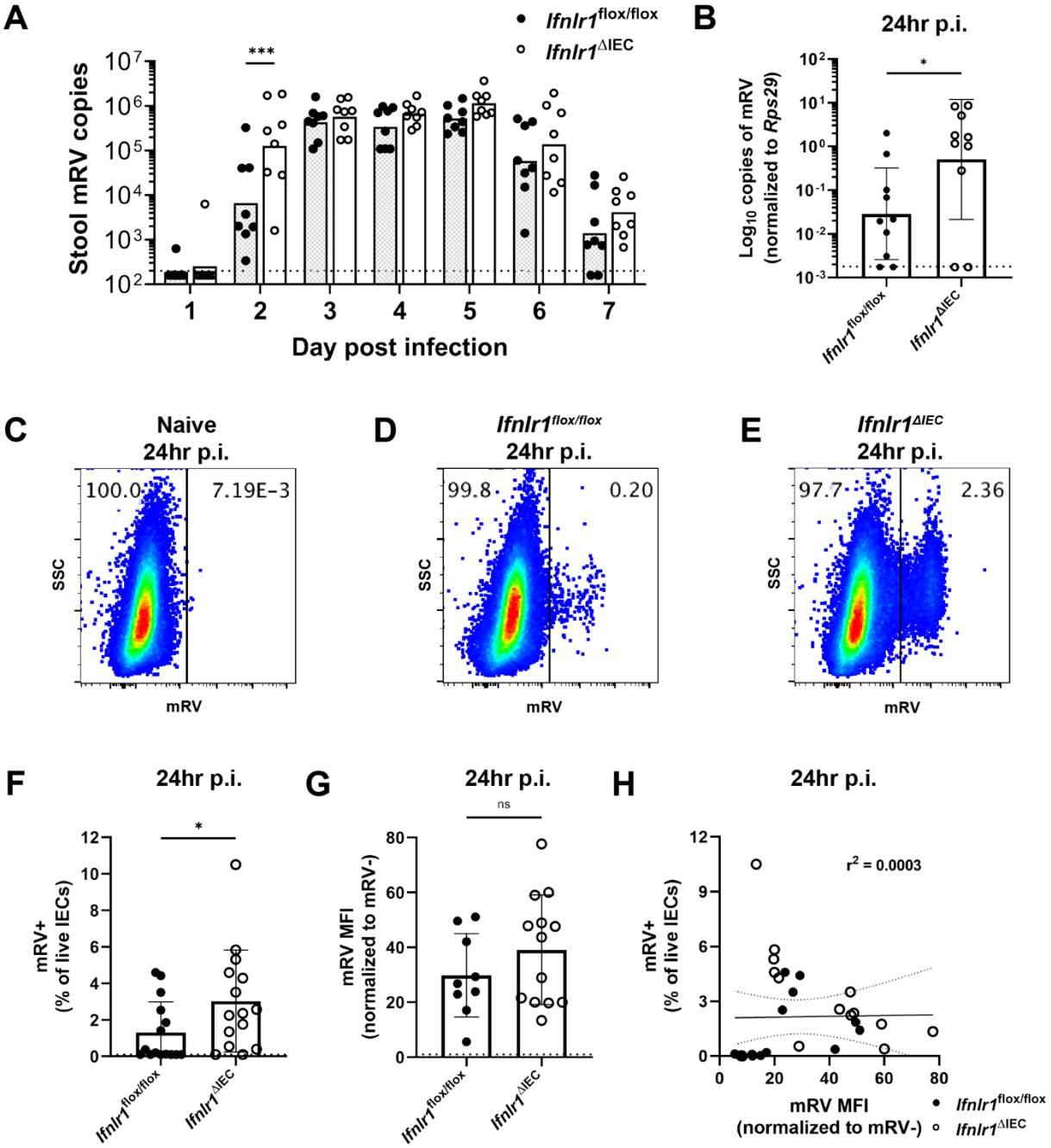

Figure 9. The homeostatic IFN-λ response preemptively protects IECs from murine rotavirus infection. *Ifnlr1*$^{flox/flox}$ and *Ifnlr1*$^{\Delta IEC}$ mice were infected with 100 SD50 **(A)** or 5000 SD50 **(B-G)** of mRV and stool **(A)** or stripped ileal intestinal epithelial cells **(B-G)** were assessed for mRV infection. **A.** Timecourse of mRV genome copies detected in the stool of *Ifnlr1*$^{flox/flox}$ and *Ifnlr1*$^{\Delta IEC}$ mice by qPCR. **B-G.** Mechanically stripped intestinal epithelial cell fractions were

analyzed by qPCR for mRV genome copies **(B)** or flow cytometry for RV antigen-positive IECs **(C-G).** Representative flow cytometry plots of naïve **(C)**, *Ifnlr1*$^{flox/flox}$ **(D)**, and *Ifnlr1*$^{\Delta IEC}$ **(E)** mice infected with mRV with quantification in **(F)**. **G.** The MFI of mRV antigen in infected cells relative to uninfected cells. **H.** A linear correlation plot of mRV+ cells and mRV MFI with 95% confidence intervals (dashed lines). Where designated in **A-G**, dashed lines = LOD as set by naïve mice. Statistical significance was determined by two-way ANOVA with Sidak's multiple comparisons **(A)**, by Mann Whitney **(B, F)**, or unpaired t-test **(G)** where * = $p < 0.05$, *** = $p < 0.001$.

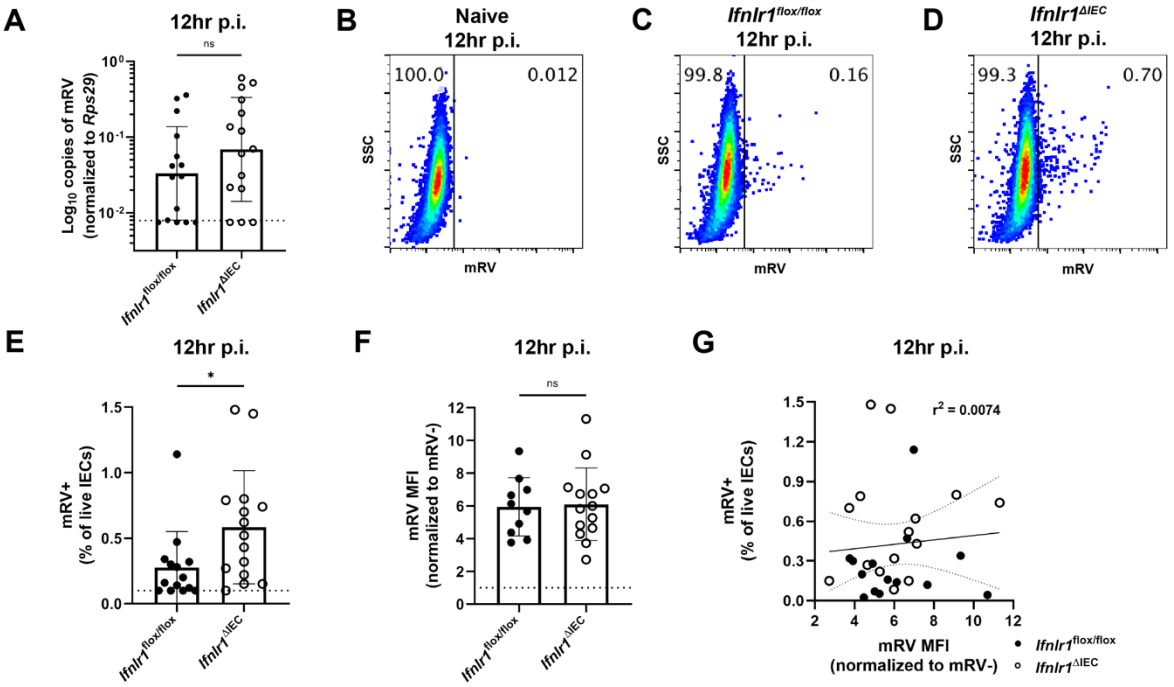

Figure S7. The homeostatic IFN-λ response preemptively protects IECs from murine rotavirus infection. *Ifnlr1*$^{flox/flox}$ and *Ifnlr1*$^{\Delta IEC}$ mice were infected with 5000 SD50 of mRV by oral gavage and stripped ileal intestinal epithelial cell fractions were analyzed by qPCR for mRV genome copies **(A)** or flow cytometry for RV antigen-positive IECs **(B-F)**. Representative flow cytometry plots of naïve **(B)**, *Ifnlr1*$^{flox/flox}$ **(C)**, and *Ifnlr1*$^{\Delta IEC}$ **(D)** mice infected with mRV. **F.** The MFI of mRV antigen in infected cells relative to uninfected cells. **G.** A linear correlation plot of mRV+

561 cells and mRV MFI with 95% confidence intervals (dashed lines). Statistical significance was
562 calculated by Mann Whitney **(A, E)**, or unpaired t-test **(F)** where * = $p < 0.05$.
563

564 **Discussion**

565 Here, we report that bacterial microbiota induce an enteric IFN-λ response in IECs at
566 homeostasis (**Figures 1-4**). This IEC-centric response is dependent on the IFN-λ receptor and
567 independent of type I IFN signaling (**Figure 3**), consistent with the dominant role of IFN-λ signaling
568 in the gastrointestinal epithelium. Furthermore, we find minimal changes in ISG expression within
569 the spleen and MLN after ABX treatment, suggesting that homeostatic ISGs are predominantly
570 expressed in the intestine. These findings differ slightly from prior descriptions of systemic type I
571 IFN responses that are dependent on bacterial microbiota (Abt et al., 2012; Bradley et al., 2019;
572 Ganal et al., 2012; Steed et al., 2017; Stefan et al., 2020; Winkler et al., 2020). However,
573 differences in the specific tissues and cell types analyzed make it difficult to draw direct
574 comparisons across these studies. Therefore, we conclude that homeostatic ISGs are
575 substantially present in IECs, but do not dispute the prior findings that relatively low homeostatic
576 ISG expression induced by type I IFN plays an important role in extra-intestinal tissues and non-
577 epithelial cell types.

578 Prior studies by Mahlakõiv et al. noted the presence of *Ifnl2/3* transcripts in CD45+ cells
579 but not EpCAM+ IECs within the intestine at homeostasis. We have confirmed these findings and
580 have extended them to show that this homeostatic expression of *Ifnl2/3*, but not homeostatic
581 expression of *Ifnb1*, is dependent on bacterial microbiota (**Figure 5**). However, we have been
582 unable to detect IFN-λ transcripts by RNA scope *in situ* hybridization in mice at homeostasis,
583 consistent with recently published data (Ingle et al., 2021). This suggests that the production of
584 IFN-λ is below our limit of detection by imaging or highly transient in nature. Swamy et al. showed
585 that T cell receptor stimulation led intraepithelial lymphocytes to produce IFN-λ (Swamy et al.,
586 2015) and Mahlakõiv et al. suggested that the primary producers of IFN-λ at steady-state are
587 intraepithelial lymphocytes. However, myeloid cells also reside near the intestinal epithelium and
588 can sample luminal contents by various mechanisms (Chieppa et al., 2006; McDole et al., 2012;
589 Niess et al., 2005). Thus, it remains to be determined which CD45+ cell types are responsible for

590 producing IFN-λ in response to stimulation by luminal MAMPs at homeostasis, but is of distinct
591 interest for future studies.

592 We initially anticipated that the distribution of homeostatic ISGs would be uniform among
593 IECs. Instead, we found that this IFN-λ response is highly localized within enteric tissues.
594 Homeostatic ISGs are observed in a minority of small intestinal villi and are primarily present in
595 mature epithelium towards the villus tips (**Figure 6**). Likewise, homeostatic ISGs are present
596 within patches of the mature epithelium in the colon (**Figure S5**). These surprising findings are
597 supported by analysis of independently-generated scRNA-seq datasets from mouse and human
598 small intestinal IECs that depict expression of homeostatic ISGs in a minority of cells with
599 predominant expression in mature enterocytes (**Figure 7**). The basis for this pattern is unknown;
600 however, it may reflect the distribution of cells capable of sensing bacterial microbiota or
601 microenvironments within the gastrointestinal tract that are particularly exposed to luminal
602 bacteria. Further delineation of the factors that render specific regions "responsive" will be of great
603 interest for follow-up studies.

604 Our finding that LPS administration or fecal transplant can partially restore the localized
605 expression of homeostatic ISGs in the small intestine (**Figures 8 and S6**) supports the concept
606 that these ISG-positive regions are uniquely exposed or responsive to bacterial MAMPs. Indeed,
607 we find that MYD88 is required for WT levels of homeostatic ISG expression in the small intestine
608 (**Figure 3**). However, MYD88 is dispensable for homeostatic ISG expression in the colon, and
609 TRIF is not required in either small intestine or colon (**Figure 3**). These data suggest that the
610 bacterial microbiota broadly stimulates homeostatic IFN-λ through multiple, redundant PRRs.
611 Furthermore, localized restoration of ISGs following LPS administration (**Figure 8**) suggests that
612 localization is an intrinsic property of homeostatic ISG stimulation. This localization may be
613 indicative of regional differences in access of luminal bacterial MAMPs to IFN-λ-producing cells.
614 One host mechanism to limit bacterial interactions with the intestinal epithelium is the presence
615 of mucus layers (Atuma et al., 2001; Johansson et al., 2011). Intriguingly, the single mucus layer

616 in the small intestine is much less adherent than the mucus layers present in the colon (Johansson
617 et al., 2011), which might allow occasional direct bacterial interactions with IECs or other cells
618 near the intestinal epithelium. However, soluble components from enteric bacteria may also
619 readily diffuse through mucus layers. In this case, there may be sporadic defects in tight junction
620 proteins that are required to maintain the intestinal epithelium. Tight junction remodeling is
621 essential to maintain intestinal integrity during apoptosis and extrusion of IECs that are regularly
622 shed from the intestinal epithelium (Williams et al., 2015). Future studies will be necessary to
623 determine whether defects in epithelial barrier integrity during extrusion events are linked to the
624 local ISG responses that we observe.

625 The signature of homeostatic ISGs in ileum tissue included well-characterized antiviral-
626 ISGs (**Figures 1-2**). These findings suggested that the homeostatic ISG response in IECs would
627 provide protection against IEC-tropic viruses, such as mRV. To investigate this question, we used
628 *Ifnlr1*$^{\Delta IEC}$ mice that lack homeostatic ISGs (**Figure 4 and 6**) rather than using ABX-treatment,
629 which introduces pleiotropic effects on rotavirus infection (Uchiyama et al., 2014) and dramatically
630 increases transit time through the intestine (Baldridge et al., 2015). Using *Ifnlr1*$^{\Delta IEC}$ mice, we found
631 increase in IEC infection by mRV at early stages of infection compared to *Ifnlr1*$^{flox/flox}$ littermates
632 (**Figure 9**). However, the protection offered by IEC expression of *Ifnlr1* was lost by the middle and
633 late stages of infection, consistent with the ability of mRV to antagonize induction of IFN
634 responses once infection is established (Arnold et al., 2013). Our observations during initiation of
635 infection may provide important context to observations in other studies that report differing
636 capacity for infection-induced IFN-λ to protect against mRV infection (Lin et al., 2016; Pott et al.,
637 2011). Ultimately, it is clear that prophylactic administration of exogenous IFN-λ protects against
638 mRV infection (Lin et al., 2016; Pott et al., 2011; Van Winkle et al., 2020), indicating that
639 homeostatic IFN-λ is also protective when induced by bacterial microbiota prior to infection. In
640 sum, these findings indicate that preexisting, homeostatic ISGs present in *Ifnlr1*-sufficient mice
641 are protective during initiation of mRV infection, but that endogenous IFN-λ does not reduce mRV

642 burden in infected cells. These data highlight the possibility that detection of bacterial microbiota
643 in particularly exposed areas may preemptively activate homeostatic ISGs as a form of
644 anticipatory immunity to protect the intestinal epithelium from enteric viruses.

645 **Methods**

646 **Mice**

647 All mice were bred using the C57BL/6 background and used within the age of 8-12 weeks;
648 C57BL/6J mice (stock # 000664) were purchased from Jackson Laboratories (Bar Harbor, ME)
649 and used as wild-type. Genetically modified mice included *Ifnlr1*$^{-/-}$ and *Ifnlr1*$^{flox/flox}$ (generated from
650 *Ifnlr1*$^{tm1a(EUCOMM)Wtsi}$ as published (Baldridge et al., 2017)), *Ifnar1*$^{-/-}$ (B6.129.Ifnar1^{tm1}), *Trif*$^{-/-}$ (JAX
651 C57BL/6J-*Ticam1*^{Lps2}/J, stock #005037), *Myd88*$^{-/-}$ (JAX B6.129P2(SJL)-*Myd88*$^{tm1.1Defr}$/J, stock
652 #009088), *Irf3*$^{-/-}$ (B6.129S/SvEv-Bcl2l12/Irf3^{tm1Ttg}), *Irf7*$^{-/}$ (B6.129P2-Irf7tm1Ttg/TtgRbrc), *Stat1*$^{-/-}$
653 (B6.129.-*Stat1*^{tm1Dlv}), and Villin-cre (B6.Cg-Tg(Vil1-cre)997Gum/J) mice. *Ifnlr1*$^{-/-}$ and *Ifnar1*$^{-/-}$ mice
654 were bred to *Ifnlr1*^{Het}/*Ifnar1*^{Het} mice to generate littermate *Ifnlr1*^{Het}/*Ifnar1*^{Het}, *Ifnlr1*^{Het}/*Ifnar1*^{KO},
655 *Ifnlr1*^{KO}/*Ifnar1*^{Het}, *Ifnlr1*^{KO}/*Ifnar1*^{KO} offspring.

656 All mice were maintained in specific-pathogen-free facilities at Oregon Health & Science
657 University (OHSU) and Washington University in St. Louis (WUSTL). Animal protocols were
658 approved by the Institutional Animal Care and Use Committee at OHSU (protocol #IP00000228)
659 and WUSTL (protocol #20190162) in accordance with standards provided in the *Animal Welfare*
660 *Act*.

661

662 **Mouse Treatments**

663 Mice were administered an *ad libitum* antibiotic cocktail consisting of: 1 g/L ampicillin, 1
664 g/L metronidazole, 1 g/L neomycin, and 0.5 g/L vancomycin (Sigma, St. Louis, MO) in autoclaved
665 H_2O (OHSU) or in 20 mg/mL grape Kool-Aid (Kraft Foods, Northfield, IL) (WUSTL). Sterile H_2O
666 (OHSU) or Kool-Aid (WUSTL) alone was used as a control. Mice were maintained on antibiotics
667 or control for 2 weeks prior to harvest.

668 Recombinant IFN-λ was provided by Bristol-Myers Squibb (New York City, NY) as a
669 monomeric conjugate comprised of 20kDa linear PEG attached to the amino-terminus of murine

670 IFN-λ. Mice were injected intraperitoneally with IFN-λ or an equal volume of PBS vehicle as
671 indicated in figure legends at the indicated time prior to analysis.
672 Mice were stimulated with of 100µg of the synthetic dsRNA analogue, poly I:C (R&D,
673 #4287) or PBS by intraperitoneal injection in a 200µL volume, 2 hours prior to harvest.
674 25µg of the bacterial product lipopolysaccharide (Sigma #L4391) or CpG (Invivogen #tlrl-
675 1585; Class A CpG oligonucleotide) were perorally administered to mice in 25µL of sterile PBS.
676 Mice were treated on days 15 and 16 of antibiotic treatment or H_2O control prior to harvest on day
677 17.
678 For transplantation of fecal material, antibiotic treatment was stopped and mice were fed
679 25uL of fecal mixture by pipet for two consecutive days. Fecal mixture was prepared by collecting
680 fecal samples from control mice; a single stool pellet was resuspended in 200uL of sterile PBS,
681 stool was broken apart by pipetting, and large particulate was allowed to settle for several minutes
682 prior to administration.
683
684 **Cell Isolation**
685 Epithelial fractions were prepared by non-enzymatic dissociation as previously described
686 (Nice et al., 2016). Briefly, mouse ileum was opened longitudinally and agitated by shaking in
687 stripping buffer (10% bovine calf serum, 15 mM HEPES, 5 mM EDTA, and 5 mM dithiothreitol
688 [DTT] in PBS) for 20 min at 37°C. Lamina propria fractions were prepared by enzymatic digestion
689 and dissociation with the Lamina Propria Dissociation Kit and GentleMacs Dissociator (Miltenyi
690 Biotec, Bergisch Gladbach, Germany). Dissociated cells were collected for use in qPCR analysis,
691 flow cytometry, and magnet enrichment.
692 **Rotavirus infection of mice**
693 Mouse rotavirus (EC strain) was graciously provided by Andrew Gewirtz (Georgia State
694 University). Viral stocks were generated by inoculating 4- to 6-day-old neonatal BALB/c mice and
695 harvesting the entire gastrointestinal tract upon presentation of diarrheal symptoms 4 to 7 days

696 later. Intestines were freeze-and-thawed, suspended in PBS, and homogenized in a bead beater
697 using 1.0-mm zirconia-silica beads (BioSpec Products). These homogenates were clarified of
698 debris, aliquoted, and stored at -70°C. The 50% shedding dose (SD50) was determined by
699 inoculation of 10-fold serial dilutions in adult C57BL/6J mice. For stool time-course studies, mice
700 were inoculated by peroral route with 100 SD50 and a single stool pellet was collected daily for
701 viral quantitation by qPCR. For protection studies, mice were inoculated by intragastric gavage
702 with 5000 SD50, and ileum was isolated and mechanically stripped 12- and 24-hours later for
703 quantitation of viral burden by qPCR and flow cytometry.
704
705 **RNA isolation, rDNA isolation, qPCR, and analysis**
706 RNA from tissue and stripped IECs was isolated with TRIzol (Life Technologies, Carlsbad,
707 CA) according to the manufacturer's protocol. RNA from magnet-enriched cells was purified by
708 Zymo *Quick*-RNA Viral Kit (Zymo Research, Irvine, CA). The larger of either 1µg of RNA or 5µL
709 of RNA were used as a template for cDNA synthesis by the ImProm-II reverse transcriptase
710 system (Promega, Madison, WI) after DNA contamination was removed with the DNAfree kit (Life
711 Technologies). 16S bacterial rDNA was isolated from stool and intestinal contents with a
712 ZymoBIOMICS DNA kit (Zymo Research, Irvine, CA) kit. Quantitative PCR was performed using
713 PerfeCTa qPCR FastMix II (QuantaBio, Beverly, MA) and the absolute quantities of transcript
714 were determined using standard curves composed of gBlocks (IDT) containing target sequences.
715 Absolute copy numbers from tissue samples were normalized to the housekeeping gene,
716 ribosomal protein S29 (*Rps29*). Taqman assays for selected genes were ordered from IDT
717 (Coralville, IA): *Rps29* (Mm.PT.58.21577577), *Ifit1* (Mm.PT.58.32674307), *Oas1a*
718 (Mm.PT.58.30459792), *Mx2* (Mm.PT.58.11386814), *Stat1* (Mm.PT.58.23792152), *Isg15*
719 (Mm.PT.58.41476392.g). Taqman assays for *Ifnl2/3* and *Ifnb1* were designed previously (Van
720 Winkle et al., 2020) and consisted of the following primer-probe sequences: *Ifnl2/3* (Primer 1 –
721 GTTCTCCCAGACCTTCAGG, Primer 2 – CCTGGGACCTGAAGCAG, Probe –

722 CCTTGCAGGCTGAGGTGGC); *Ifnb1* (Primer 1 – CTCCAGCTCCAAGAAAGGAC, Primer 2 –
723 GCCCTGTAGGTGAGGTTGAT, Probe – CAGGAGCTCCTGGAGCAGCTGA). Murine rotavirus
724 was detected using Taqman primer-probe sets specific for 422-521 of GeneBank sequence
725 DQ391187 as previously described (Fenaux et al., 2006) with the following sequences: Primer 1
726 – GTTCGTTGTGCCTCATTCG, Primer 2 – TCGGAACGTACTTCTGGAC, Probe –
727 AGGAATGCTTCAGCGCTG; and universal bacterial 16S rDNA was detected using Taqman
728 primer-probe sets with previously designed sequences (Nadkarni et al., 2002): Primer 1 –
729 GGACTACCAGGGTATCTAATCCTGTT, Primer 2 – TCCTACGGGAGGCAGCAGT, Probe –
730 CGTATTACCGCGGCTGCTGGCAC.
731

732 **RNAscope**

733 Swiss rolls of intestinal tissue were fixed in 10% neutral-buffered formalin for 18-24hr and
734 paraffin-embedded. Tissue sections (5μm) were cut and maintained at room temperature with
735 desiccant until staining. RNA *in situ* hybridization was performed using the RNAscope Multiplex
736 Fluorescent v2 kit (Advanced Cell Diagnostics, Newark, CA) per protocol guidelines. Staining with
737 anti-sense probes for detection of *Ifit1* (ACD, #500071-C2) and *Usp18* (ACD, #524651) was
738 performed using ACDBio protocols and reagents. Slides were stained with DAPI and mounted
739 with ProLong Gold antifade reagent (ThermoFisher), and imaged using a Zeiss ApoTome2 on an
740 Axio Imager, with a Zeiss AxioCam 506 (Zeiss).

741 **Flow cytometry and Magnet Enrichment**

742 Dissociated cells were collected and stained for flow cytometry. Cells were stained with
743 Zombie Aqua viability dye (BioLegend), Fc receptor-blocking antibody (CD16/CD32; BioLegend),
744 anti-EpCAM (clone G8.8; BioLegend), and anti-CD45 (clone 30-F11; BioLegend). For analysis of
745 murine rotavirus infection, cells were stained with anti-rotavirus (polyclonal; ThermoFisher, #PA1-
746 7241) followed by goat anti-rabbit secondary (ThermoFisher). All data were analyzed using
747 FlowJo software (BD Biosciences). Gates were set based on unstained and single-fluorophore

748 stains. IECs were selected by gating on live, EpCAM-positive, CD45-negative cells. Gates for
749 murine rotavirus infection were set based on naïve samples.

750 Where indicated, dissociated cells were enriched using MojoSort Mouse anti-APC
751 Nanobeads (BioLegend, #480072) after flow cytometry staining for anti-EpCAM and anti-CD45
752 with APC fluorophores by following manufacturer protocols.

753

754 **RNA sequencing and expression analysis**

755 Wild-type C57BL/6J or *Ifnlr1*$^{-/-}$ mice were administered *ad libitum* Kool-aid or ABX for two
756 weeks, or wild-type mice were administered 25μg recombinant IFN-λ for one day, then ileal
757 segments lacking Peyer's patches were harvested and RNA sequencing was performed as prior
758 (Park et al., 2016). mRNA from ilea was purified with oligo-dT beads (Invitrogen, Carlsbad, CA)
759 and cDNA was synthesized using a custom oligo-dT primer containing a barcode and adaptor-
760 linker sequence, degradation of RNA-DNA hybrid following single-strand synthesis, and ligation
761 of a second sequencing linker with T4 ligase (New England Biolabs, Ipswich, MA). These
762 reactions were cleaned up by solid phase reversible immobilization (SPRI), followed by
763 enrichment by PCR and further SPRI to yield strand-specific RNA-seq libraries. Libraries were
764 sequenced with an Illumina HiSeq 2500 with three to four mice were included in each group.
765 Samples were demultiplexed with second mate, reads were aligned with STAR aligner and then
766 counted with HT-Seq. Differentially expressed genes were identified using DESeq2 (Love et al.,
767 2014) based on cutoffs of 2-fold change, and an inclusive p-value < 0.5. Standard gene set
768 enrichment analysis was performed to identify enrichments in IFN-λ response genes. RNA-seq
769 data were uploaded to the European Nucleotide Archive (accession #: PRJEB43446).

770

771 **Statistical Analyses**

772 Data were analyzed with Prism software (GraphPad Prism Software), with specified tests
773 as noted in the figure legends.

774

775 **Data availability.**

776 RNA sequencing data obtained in this study have been deposited in the European
777 Nucleotide Archive (accession #: PRJEB43446).

778

779 **Acknowledgments**

780 The authors would like to thank the following OHSU core facilities: Integrated Genomics
781 Laboratory, Advanced Light Microscopy Core, and Histopathology Core; and the following
782 WUSTL core facilities: Genome Technology Access Center. T.J.N. was supported NIH grant R01-
783 AI130055 and by a faculty development award from the Sunlin & Priscilla Chou Foundation. J.A.V.
784 was supported by NIH grants T32-GM071338 and T32-AI007472. M.T.B. was supported by NIH
785 grants R01-AI139314, R01-AI141716, and R01-AI141478, the Pew Biomedical Scholars Program
786 of the Pew Charitable Trusts, and a Children's Discovery Institute of Washington University and
787 St. Louis Children's Hospital Interdisciplinary Research Initiative grant (MI-II-2019–790). The
788 funders had no role in study design, data collection and interpretation, or the decision to submit
789 the work for publication.

790

791 **Author Contributions**

792 Conceptualization, J.A.V., M.T.B., and T.J.N.; Methodology, J.A.V., M.T.B., and T.J.N.;
793 Investigation, J.A.V., S.T.P., E.A.K., M.W., H.I., C.D., D.C., A.W., M.A., S.L., and T.J.N.; Writing
794 – Original Draft, J.A.V.; Writing – Review & Editing, J.A.V., M.T.B., and T.J.N.; Visualization,
795 J.A.V.; Supervision, M.T.B. and T.J.N.; Project Administration, L.L., M.T.B., and T.J.N.; Funding
796 Acquisition, M.T.B. and T.J.N.

797

798 **Disclosure**

799 We declare no competing interests.

800 **References**

801 Abt, M.C., Osborne, L.C., Monticelli, L.A., Doering, T.A., Alenghat, T., Sonnenberg, G.F., Paley,
802 M.A., Antenus, M., Williams, K.L., Erikson, J., et al. (2012). Commensal bacteria calibrate the
803 activation threshold of innate antiviral immunity. Immunity *37*, 158–170.

804 Arnold, M.M., Sen, A., Greenberg, H.B., and Patton, J.T. (2013). The battle between rotavirus
805 and its host for control of the interferon signaling pathway. PLoS Pathog. *9*, e1003064.

806 Atuma, C., Strugala, V., Allen, A., and Holm, L. (2001). The adherent gastrointestinal mucus gel
807 layer: thickness and physical state in vivo. Am. J. Physiol. Gastrointest. Liver Physiol. *280*,
808 G922-9.

809 Baldridge, M.T., Nice, T.J., McCune, B.T., Yokoyama, C.C., Kambal, A., Wheadon, M.,
810 Diamond, M.S., Ivanova, Y., Artyomov, M., and Virgin, H.W. (2015). Commensal microbes and
811 interferon-λ determine persistence of enteric murine norovirus infection. Science *347*, 266–269.

812 Baldridge, M.T., Lee, S., Brown, J.J., McAllister, N., Urbanek, K., Dermody, T.S., Nice, T.J., and
813 Virgin, H.W. (2017). Expression of Ifnlr1 on Intestinal Epithelial Cells Is Critical to the Antiviral
814 Effects of Interferon Lambda against Norovirus and Reovirus. J. Virol. *91*, JVI.02079-16.

815 Bradley, K.C., Finsterbusch, K., Schnepf, D., Crotta, S., Llorian, M., Davidson, S., Fuchs, S.Y.,
816 Staeheli, P., and Wack, A. (2019). Microbiota-Driven Tonic Interferon Signals in Lung Stromal
817 Cells Protect from Influenza Virus Infection. Cell Rep. *28*, 245-256.e4.

818 Burns, J.W., Krishnaney, A.A., Vo, P.T., Rouse, R. V., Anderson, L.J., and Greenberg, H.B.
819 (1995). Analyses of homologous rotavirus infection in the mouse model. Virology *207*, 143–153.

820 Chieppa, M., Rescigno, M., Huang, A.Y.C., and Germain, R.N. (2006). Dynamic imaging of
821 dendritic cell extension into the small bowel lumen in response to epithelial cell TLR
822 engagement. J. Exp. Med. *203*, 2841–2852.

823 Chu, H., and Mazmanian, S.K. (2013). Innate immune recognition of the microbiota promotes
824 host-microbial symbiosis. Nat. Immunol. *14*, 668–675.

825 Elmentaite, R., Ross, A.D.B., Roberts, K., James, K.R., Ortmann, D., Gomes, T., Nayak, K.,
826 Tuck, L., Pritchard, S., Bayraktar, O.A., et al. (2020). Single-Cell Sequencing of Developing
827 Human Gut Reveals Transcriptional Links to Childhood Crohn's Disease. Dev. Cell *55*, 771-
828 783.e5.

829 Fenaux, M., Cuadras, M.A., Feng, N., Jaimes, M., and Greenberg, H.B. (2006). Extraintestinal
830 spread and replication of a homologous EC rotavirus strain and a heterologous rhesus rotavirus
831 in BALB/c mice. J. Virol. *80*, 5219–5232.

832 Ganal, S.C., Sanos, S.L., Kallfass, C., Oberle, K., Johner, C., Kirschning, C., Lienenklaus, S.,
833 Weiss, S., Staeheli, P., Aichele, P., et al. (2012). Priming of natural killer cells by nonmucosal
834 mononuclear phagocytes requires instructive signals from commensal microbiota. Immunity *37*,
835 171–186.

836 Haber, A.L., Biton, M., Rogel, N., Herbst, R.H., Shekhar, K., Smillie, C., Burgin, G., Delorey,
837 T.M., Howitt, M.R., Katz, Y., et al. (2017). A single-cell survey of the small intestinal epithelium.
838 Nature *551*, 333–339.

839 Hernández, P.P., Mahlakoiv, T., Yang, I., Schwierzeck, V., Guendel, F., Gronke, K., Ryffel, B.,
840 Dumoutier, L., Renauld, J., and Suerbaum, S. (2015). Interferon-λ and interleukin-22 cooperate
841 for the induction of interferon-stimulated genes and control of rotavirus infection. Nat. Immunol.
842 *16*, 698–707.

843 Honda, K., and Littman, D.R. (2016). The microbiota in adaptive immune homeostasis and

disease. Nature *535*, 75–84.

Honda, K., Yanai, H., Negishi, H., Asagiri, M., Sato, M., Mizutani, T., Shimada, N., Ohba, Y., Takaoka, A., Yoshida, N., et al. (2005a). IRF-7 is the master regulator of type-I interferon-dependent immune responses. Nature *434*, 772–777.

Honda, K., Ohba, Y., Yanai, H., Negishi, H., Mizutani, T., Takaoka, A., Taya, C., and Taniguchi, T. (2005b). Spatiotemporal regulation of MyD88-IRF-7 signalling for robust type-I interferon induction. Nature *434*, 1035–1040.

Ingle, H., Peterson, S.T., and Baldridge, M.T. (2018). Distinct Effects of Type I and III Interferons on Enteric Viruses. Viruses *10*.

Ingle, H., Hassan, E., Gawron, J., Mihi, B., Li, Y., Kennedy, E.A., Kalugotla, G., Makimaa, H., Lee, S., Desai, P., et al. (2021). Murine astrovirus tropism for goblet cells and enterocytes facilitates an IFN-λ response in vivo and in enteroid cultures. Mucosal Immunol. *14*, 751–761.

Iwasaki, A., and Medzhitov, R. (2015). Control of adaptive immunity by the innate immune system. Nat. Immunol. *16*, 343–353.

Johansson, M.E. V., Larsson, J.M.H., and Hansson, G.C. (2011). The two mucus layers of colon are organized by the MUC2 mucin, whereas the outer layer is a legislator of host-microbial interactions. Proc. Natl. Acad. Sci. *108*, 4659–4665.

Kim, S., Covington, A., and Pamer, E.G. (2017). The intestinal microbiota: Antibiotics, colonization resistance, and enteric pathogens. Immunol. Rev. *279*, 90–105.

Kotenko, S. V, and Durbin, J.E. (2017). Contribution of type III interferons to antiviral immunity: Location, Location, Location. J. Biol. Chem. *292*, 7295–7303.

Krajmalnik-Brown, R., Ilhan, Z.E., Kang, D.W., and DiBaise, J.K. (2012). Effects of gut microbes on nutrient absorption and energy regulation. Nutr. Clin. Pract. *27*, 201–214.

Lee, S., Liu, H., Wilen, C.B., Sychev, Z.E., Desai, C., Hykes, B.L., Orchard, R.C., McCune, B.T., Kim, K.-W., Nice, T.J., et al. (2019). A Secreted Viral Nonstructural Protein Determines Intestinal Norovirus Pathogenesis. Cell Host Microbe *25*, 845-857.e5.

Levy, D.E., and García-Sastre, A. (2001). The virus battles: IFN induction of the antiviral state and mechanisms of viral evasion. Cytokine Growth Factor Rev. *12*, 143–156.

Lin, J.-D., Feng, N., Sen, A., Balan, M., Tseng, H.-C., McElrath, C., Smirnov, S. V., Peng, J., Yasukawa, L.L., Durbin, R.K., et al. (2016). Distinct Roles of Type I and Type III Interferons in Intestinal Immunity to Homologous and Heterologous Rotavirus Infections. PLoS Pathog. *12*, e1005600.

Love, M.I., Huber, W., and Anders, S. (2014). Moderated estimation of fold change and dispersion for RNA-seq data with DESeq2. Genome Biol. *15*, 550.

Mahlakõiv, T., Hernandez, P., Gronke, K., Diefenbach, A., and Staeheli, P. (2015). Leukocyte-derived IFN-α/β and epithelial IFN-λ constitute a compartmentalized mucosal defense system that restricts enteric virus infections. PLoS Pathog. *11*, e1004782.

McDole, J.R., Wheeler, L.W., McDonald, K.G., Wang, B., Konjufca, V., Knoop, K.A., Newberry, R.D., and Miller, M.J. (2012). Goblet cells deliver luminal antigen to CD103 + dendritic cells in the small intestine. Nature *483*, 345–349.

Monroe, K.M., McWhirter, S.M., and Vance, R.E. (2010). Induction of type I interferons by bacteria. Cell. Microbiol. *12*, 881–890.

Nadkarni, M., Martin, F.E., Jacques, N.A., and Hunter, N. (2002). Determination of bacterial load by real-time PCR using a broad range (universal) probe and primer set. Microbiology *148*, 257–

888 266.

889 Nice, T.J., Baldridge, M.T., McCune, B.T., Norman, J.M., Lazear, H.M., Artyomov, M., Diamond,
890 M.S., and Virgin, H.W. (2015). Interferon-λ cures persistent murine norovirus infection in the
891 absence of adaptive immunity. Science *347*, 269–273.

892 Nice, T.J., Osborne, L.C., Tomov, V.T., Artis, D., Wherry, E.J.J., and Virgin, H.W. (2016). Type I
893 Interferon Receptor Deficiency in Dendritic Cells Facilitates Systemic Murine Norovirus
894 Persistence Despite Enhanced Adaptive Immunity. PLoS Pathog. *12*, e1005684.

895 Niess, J.H., Brand, S., Gu, X., Landsman, L., Jung, S., McCormick, B.A., Vyas, J.M., Boes, M.,
896 Ploegh, H.L., Fox, J.G., et al. (2005). CX3CR1-mediated dendritic cell access to the intestinal
897 lumen and bacterial clearance. Science *307*, 254–258.

898 Odendall, C., Voak, A.A., and Kagan, J.C. (2017). Type III IFNs Are Commonly Induced by
899 Bacteria-Sensing TLRs and Reinforce Epithelial Barriers during Infection. J. Immunol. *199*,
900 3270–3279.

901 Osterlund, P.I., Pietilä, T.E., Veckman, V., Kotenko, S. V, and Julkunen, I. (2007). IFN
902 regulatory factor family members differentially regulate the expression of type III IFN (IFN-
903 lambda) genes. J. Immunol. *179*, 3434–3442.

904 Park, S., Buck, M.D., Desai, C., Zhang, X., Loginicheva, E., Martinez, J., Freeman, M.L., Saitoh,
905 T., Akira, S., Guan, J.L., et al. (2016). Autophagy Genes Enhance Murine Gammaherpesvirus
906 68 Reactivation from Latency by Preventing Virus-Induced Systemic Inflammation. Cell Host
907 Microbe *19*, 91–101.

908 Pott, J., Mahlakoiv, T., Mordstein, M., Duerr, C.U., Michiels, T., Stockinger, S., Staeheli, P., and
909 Hornef, M.W. (2011). IFN-λ determines the intestinal epithelial antiviral host defense. Proc. Natl.
910 Acad. Sci. *108*, 7944–7949.

911 Rojas, J.M., Alejo, A., Martín, V., and Sevilla, N. (2021). Viral pathogen-induced mechanisms to
912 antagonize mammalian interferon (IFN) signaling pathway. Cell. Mol. Life Sci. *78*, 1423–1444.

913 Rooks, M.G., and Garrett, W.S. (2016). Gut microbiota, metabolites and host immunity. Nat.
914 Rev. Immunol. *16*, 341–352.

915 Sadler, A.J., and Williams, B.R.G. (2008). Interferon-inducible antiviral effectors. Nat. Rev.
916 Immunol. *8*, 559–568.

917 Schmid, S., Mordstein, M., Kochs, G., García-Sastre, A., and TenOever, B.R. (2010).
918 Transcription factor redundancy ensures induction of the antiviral state. J. Biol. Chem. *285*,
919 42013–42022.

920 Schneider, W.M., Chevillotte, M.D., and Rice, C.M. (2014). Interferon-stimulated genes: a
921 complex web of host defenses. Annu. Rev. Immunol. *32*, 513–545.

922 Schoggins, J.W., and Rice, C.M. (2011). Interferon-stimulated genes and their antiviral effector
923 functions. Curr. Opin. Virol. *1*, 519–525.

924 Sommereyns, C., Paul, S., Staeheli, P., and Michiels, T. (2008). IFN-Lambda (IFN-λ) Is
925 Expressed in a Tissue-Dependent Fashion and Primarily Acts on Epithelial Cells In Vivo. PLoS
926 Pathog. *4*, e1000017.

927 Steed, A.L., Christophi, G.P., Kaiko, G.E., Sun, L., Goodwin, V.M., Jain, U., Esaulova, E.,
928 Artyomov, M.N., Morales, D.J., Holtzman, M.J., et al. (2017). The microbial metabolite
929 desaminotyrosine protects from influenza through type I interferon. Science (80-.). *357*, 498–
930 502.

931 Stefan, K.L., Kim, M. V, Iwasaki, A., and Kasper, D.L. (2020). Commensal Microbiota

932 Modulation of Natural Resistance to Virus Infection. Cell *183*, 1312-1324.e10.

933 Stockinger, S., Duerr, C.U., Fulde, M., Dolowschiak, T., Pott, J., Yang, I., Eibach, D., Bäckhed,
934 F., Akira, S., Suerbaum, S., et al. (2014). TRIF signaling drives homeostatic intestinal epithelial
935 antimicrobial peptide expression. J. Immunol. *193*, 4223–4234.

936 Swamy, M., Abeler-Dörner, L., Chettle, J., Mahlakõiv, T., Goubau, D., Chakravarty, P., Ramsay,
937 G., Reis e Sousa, C., Staeheli, P., Blacklaws, B.A., et al. (2015). Intestinal intraepithelial
938 lymphocyte activation promotes innate antiviral resistance. Nat. Commun. *6*, 7090.

939 Taylor, K.E., and Mossman, K.L. (2013). Recent advances in understanding viral evasion of
940 type I interferon. Immunology *138*, 190–197.

941 Thompson, M.R., Kaminski, J.J., Kurt-Jones, E.A., and Fitzgerald, K.A. (2011). Pattern
942 recognition receptors and the innate immune response to viral infection. Viruses *3*, 920–940.

943 Tomasello, E., Naciri, K., Chelbi, R., Bessou, G., Fries, A., Gressier, E., Abbas, A., Pollet, E.,
944 Pierre, P., Lawrence, T., et al. (2018). Molecular dissection of plasmacytoid dendritic cell
945 activation in vivo during a viral infection. EMBO J. *37*, 1–19.

946 Uchiyama, R., Chassaing, B., Zhang, B., and Gewirtz, A.T. (2014). Antibiotic treatment
947 suppresses rotavirus infection and enhances specific humoral immunity. J. Infect. Dis. *210*,
948 171–182.

949 Williams, J.M., Duckworth, C.A., Burkitt, M.D., Watson, A.J.M., Campbell, B.J., and Pritchard,
950 D.M. (2015). Epithelial cell shedding and barrier function: a matter of life and death at the small
951 intestinal villus tip. Vet. Pathol. *52*, 445–455.

952 Van Winkle, J.A., Constant, D.A., Li, L., and Nice, T.J. (2020). Selective Interferon Responses
953 of Intestinal Epithelial Cells Minimize Tumor Necrosis Factor Alpha Cytotoxicity. J. Virol. *94*,
954 e00603-20.

955 Winkler, E.S., Shrihari, S., Hykes, B.L., Handley, S.A., Andhey, P.S., Huang, Y.-J.S., Swain, A.,
956 Droit, L., Chebrolu, K.K., Mack, M., et al. (2020). The Intestinal Microbiome Restricts Alphavirus
957 Infection and Dissemination through a Bile Acid-Type I IFN Signaling Axis. Cell *182*, 901-
958 918.e18.

959